

University of Central Florida

STARS

Electronic Theses and Dissertations, 2020-

2020

Copper/N-acetylcysteine Coated Iron Oxide Nanoparticles Synthesis, Characterization, and Antimicrobial Activities

Danya Belnour

University of Central Florida



Part of the [Medical Biotechnology Commons](#)

Find similar works at: <https://stars.library.ucf.edu/etd2020>

University of Central Florida Libraries <http://library.ucf.edu>

This Masters Thesis (Open Access) is brought to you for free and open access by STARS. It has been accepted for inclusion in Electronic Theses and Dissertations, 2020- by an authorized administrator of STARS. For more information, please contact STARS@ucf.edu.

STARS Citation

Belnour, Danya, "Copper/N-acetylcysteine Coated Iron Oxide Nanoparticles Synthesis, Characterization, and Antimicrobial Activities" (2020). *Electronic Theses and Dissertations, 2020-*. 174.

<https://stars.library.ucf.edu/etd2020/174>

COPPER/ N-ACETYLCYSTEINE COATED IRON OXIDE NANOPARTICLES
SYNTHESIS, CHARACTERIZATION, AND ANTIMICROBIAL ACTIVITY

By

DANYA BELNOUR
B.S. University of Central Florida, 2018

A thesis submitted in partial fulfillment of the requirements
for the degree of Master of Science
in the Burnett School of Biomedical Sciences
in the College of Medicine
at the University of Central Florida
Orlando, Florida

Summer Term
2020

Major Professor: Swadeshmukul Santra

© 2020 Danya Belnour

ABSTRACT

In recent years, there is a growing interest in developing metal based antimicrobial nanomaterials suitable for agricultural and biomedical applications. For centuries, Copper (Cu) biocide has been used for protecting a wide variety of crops from devastating bacterial and fungal diseases. However, prolonged and aggressive use of Cu led to the development of resistance and accumulation in soil. The latter has been linked to aquatic toxicity due to soil Cu leaching. Furthermore, copper build up in soil causes phytotoxicity and reduces uptake of micronutrient Zn through the root system. In biomedical field, Cu has been historically used as an antimicrobial agent in wound dressing. In healthcare facilities, Cu based touch surfaces are shown to significantly reduce antimicrobial infection rates. Emerging biomedical applications include wound healing, sensing and even potential use of nano-Cu as cancer therapeutic. However, Cu cytotoxicity is a serious concern. There is a strong need for developing advanced Cu based composite material that will retain antimicrobial properties as reduced Cu load until a suitable alternative becomes available. In this thesis, the objective is to develop a Cu coated Iron Oxide nanocomposite. The idea is to distribute Cu over the high surface area of biocompatible Iron Oxide nanoparticle (IONP) to improve Cu bioavailability. In the design of Cu-IONP nanocomposite, we have introduced N-Acetyl Cysteine (NAC, an antioxidant biomolecule) that anchors IONP to Cu. The composite was synthesized using a co-precipitation technique. Characterization of the Cu/NAC-IONP nanocomposite was done using Atomic Absorption Spectroscopy (AAS), Dynamic Light Scattering, Fourier Transform Infrared Spectroscopy (FTIR), Scanning electron microscopy and X-Ray Photoelectron Spectroscopy. Characterization

results support the formation of composite and NAC as a bidentate ligand conjugating Cu to IONP. Antimicrobial activity of Cu/NAC-IONP nanocomposite was studied using ASTM published protocol. The Cu/NAC-IONP nanocomposite shows higher Colony Forming Unit Percent reduction when compared with NAC-Iron Oxide and no treatment. This suggests that antimicrobial activity of Cu is retained in the nanocomposite. Additionally, AAS study revealed an interesting property of the nanocomposite that the Cu release is strongly dependent on incubation temperature. Cu ion release is increased with the increase in incubation temperature. This new finding may lead to design of a delivery system where Cu release can be controlled by tuning temperature.

This thesis is dedicated to my loving parents Iman Tunali and Khalid Banur, and my siblings Mohammed, Seraj and Shehab Belnour. Your infinite love and support are the drive the keeps me going. I am grateful for each one of you.

ACKNOWLEDGMENTS

First and Foremost, my deepest gratitude goes to Dr. Maria Campos. Her sincere mentorship through explaining concepts in material chemistry, recommendation of experiment design, and data analysis training are the reason this project is possible. Thank you for continues support, guidance, and advice. I am honored and proud to have been one of your mentees. Also, my sincerest and deepest thanks to my thesis adviser Dr. Swadeshmukul Santra for this amazing opportunity and guidance. I am grateful to have had the opportunity to learn from you and be part of your group. Thank you to my thesis committee member Dr. Ellen Kang and Dr. Michal Masternak for their kindness, support and valuable advice throughout the projects. In addition, I would like to thank Dr. Hajeewaka Mendis for Microbiology training, and Dr. Matthew Rex for Atomic Absorption Spectroscopy and FTIR instrument training. I am thankful to all my lab mates, teachers, and friends for their support and encouragements through the years. Finally, thank you to Material characterization Facility (MCF) and NanoScience Technology Center (NSTC) at the University of Central Florida for characterization instruments access and instrument training. I would like to acknowledge the Citrus Research and Development Foundation (CRDF project # 18-020) for providing partial support and the UCF Materials Innovation for Sustainable Agriculture (MISA) center for the technical support.

TABLE OF CONTENTS

LIST OF FIGURES	ix
LIST OF TABLES	xii
LIST OF ABBREVIATIONS.....	xiii
CHAPTER ONE: INTRODUCTION.....	1
1.1: Nanotechnology in Agriculture	1
1.2: Antimicrobial Nanomaterials for Agriculture Purposes	2
1.3: Nanomaterial Design	4
1.3.1: Iron Oxide Nanomaterial	5
1.3.2: Copper and N-acetylcysteine Nanomaterial Coating.....	7
CHAPTER TWO: NANOMATERIALS CHARACTERIZATION	12
2.1: Characterizations Techniques	12
2.1.1: Atomic Absorption Spectroscopy (AAS)	13
2.1.2: Dynamic Light Scattering (DLS).....	14
2.1.3: Fourier Transform Infrared Spectroscopy (FTIR)	15
2.1.4: Scanning Electron Microscopy (SEM)	15
2.1.5: X-ray Photoelectron Spectroscopy (XPS)	16
CHAPTER THREE: METHODOLOGY	17
3.1: Nanomaterial Synthesis Procedure	17
3.1.1: Iron Oxide Nanoparticle (IONP) Preparation	17
3.1.2: N-acetylcysteine-Iron Oxide Nanoparticle (NAC-IONP) Preparation	18

3.1.3: Copper/N-acetylcysteine- Iron oxide Nanoparticle (Cu/NAC-IONP) Preparation	19
3.2: Antimicrobial Studies	23
3.2.1: Determination of Antimicrobial Activity of Nanomaterials	23
3.2.1.A: Antimicrobial Activity of NAC-IONP and Cu/NAC-IONP on <i>Escherichia coli</i>	24
3.2.1.B: Antimicrobial Activity of NAC-IONP and Cu/NAC-IONP on <i>Pseudomonas syringea</i>	25
3.2.2: Quantification of Copper Release.....	26
CHAPTER FOUR: RESULTS & DISCUSSION.....	28
CHAPTER FIVE: CONCLUSION.....	55
APPENDIX: SUPPLEMENTERY INFORMATION	56
LIST OF REFERENCES	61

LIST OF FIGURES

Figure 1: Nanomaterial design and possible interaction of molecules. A: Iron oxide (IONP), B: N-Acetylcysteine-Iron Oxide (NAC-IONP) and Copper/N-acetylcysteine-Iron Oxide (Cu/NAC-IONP). “Created with BioRender.com.”	11
Figure 2: A simplified illustration of the synthesis procedure completed to produce IONP. “Created with BioRender.com.”	21
Figure 3: A simplified visual illustration of the synthesis procedure taken to produce NAC-IONP. “Created with BioRender.com.”	22
Figure 4: A simplified illustration of the synthesis procedure of Cu/NAC-IONP “Created with BioRender.com.”	23
Figure 5: A simplified illustration of the steps taken to investigate the antimicrobial activity of NAC-IONP and Cu/NAC-IONP “Created with BioRender.com.”	26
Figure 6: An illustration of procedure taken to calculate copper release in the media following 24-hour incubation. “Created with BioRender.com.”	27
Figure 7: DLS analysis of Iron Oxide nanomaterials before freeze drying.	31
Figure 8: DLS analysis of NAC-Iron Oxide before freeze drying.	32
Figure 9: DLS analysis of Cu/NAC-Iron Oxide before freeze drying.	33
Figure 10: Hydrodynamic size comparison between Iron oxide, NAC-iron oxide, and Cu/NAC-Iron Oxide.	34
Figure 11: FTIR spectrum of Iron Oxide nanomaterial.	36
Figure 12: FTIR spectrum of NAC-Iron Oxide.	37

Figure 13: FTIR spectrum of Cu/NAC-Iron Oxide nanomaterial.	38
Figure 14: SEM images of Iron Oxide nanoparticle.	40
Figure 15: SEM Images of NAC-Iron Oxide.....	41
Figure 16: SEM Images of NAC-Iron Oxide.....	42
Figure 17: SEM Images of Cu/NAC-Iron Oxide.....	43
Figure 18: SEM-EDS of Iron Oxide nanoparticle.	44
Figure 19: Energy Dispersive X-Ray Spectroscopy (EDS) of NAC-IONP.	45
Figure 20: Energy Dispersive X-Ray Spectroscopy (EDS) of Cu/NAC-IONP.....	46
Figure 21: Examine the reduction of Cell Colony Count after 0 hours, 4 Hours and 24 Hours of NAC-Iron Oxide and Copper-NAC-iron Oxide compare with No treatment (NT). The data of nanomaterials treatment using <i>Escherichia coli</i> as animal infecting bacteria model system.	48
Figure 22: Examine the reduction of Cell Colony Count after 0 hours, 4 Hours and 24 Hours of NAC-Iron Oxide and Copper-NAC-iron Oxide compare with No treatment (NT) Shows the data for nanomaterials treatment using <i>Pseudomonas syringea</i> as a plant infecting bacteria model system.	49
Figure 23: AAS study of Copper release in LB media.	52
Figure 24: AAS study of Copper Release in NB media.	53
Figure 25: An XPS survey spectrum of IONP.....	58
Figure 26: An XPS survey spectrum of NAC-IONP	59
Figure 27: An XPS survey spectrum of Cu/NAC-IONP	60

LIST OF TABLES

Table 1: List of reagents utilized for the synthesis of nanomaterials.	17
Table 2: Atomic Absorption Spectroscopy Analysis and the calculations of weight percentage (Wt%) of total Iron and total Copper in each synthesized nanomaterial including Iron Oxide, NAC-Iron Oxide, and Copper/NAC-Iron Oxide.....	29
Table 3: Summary of DLS analysis including the Z-Average, Polydispersity Index (PDI), count rate and pH of the three synthesized nanomaterials Iron oxide, NAC-Iron Oxide, and Cu/NAC-Iron oxide	33
Table 4: Iron Oxide FTIR assigned peaks and their recognized chemical and previously identified similar peaks in the literature.....	36
Table 5: FTIR assigned peaks, their recognized chemical bond and previously identified peaks in the literature for NAC-IONP and Cu/NAC-IONP.....	39
Table 6: Semi-quantitative results of SEM-EDS analysis.	44
Table 7: SEM-EDS semi-quantitative analysis of NAC-IONP.....	45
Table 8: SEM-EDS semi-quantitative analysis of Cu/NAC-IONP	46
Table 9: Percent reduction of bacterial titer and the Log ₁₀ bacterial titer reduction for the NAC-Iron Oxide and Cu/NAC-iron Oxide treatments after 24 hours of incubation.	50
Table 10: Effects of temperature on the Copper release amount after 24 hours of incubation. ...	51

LIST OF ABBREVIATIONS

Copper- Cu

Copper/ N- Acetylcysteine- Iron Oxide nanoparticles - Cu/NAC-IONP

Iron Oxide Nanoparticles – IONP

N- Acetylcysteine- NAC

N- Acetylcysteine- Iron Oxide nanoparticles -NAC-IONP

CHAPTER ONE: INTRODUCTION

1.1: Nanotechnology in Agriculture

Nanomaterial is defined as any materials, devices and structures that has dimension in the Nano scale or 10^{-9} in SI units (Kalantar-zadeh & Fry, 2007). Nanotechnology deals with nanometer scale (1-100 nanometers) science, engineering, and technology. By definition, nanomaterial will have at least one dimension in the nanometer scale. Nanotechnology utilize the unique chemical, physical, and biological properties when compared to the bulk materials. Also, nanotechnology is a multidisciplinary field, it encompassed many disciplines of science such as, chemistry, physics, biology, engineering, and many others. This interdisciplinary field aims at creating and developing materials, devices, and systems that take advantage of the unique properties of nanomaterials. Today, many researchers are working to develop nanomaterials and nanodevices that could be useful as antimicrobial agents, agriculture biocide, drug delivery, anticancer treatment, and biomedical image contrast agents.

However, nanomaterial is being widely investigated in agriculture and in all stages of product development such as, packaging, storing and transport (M. A. Ali et al., 2014) One of the main concerns for nanotechnology in agriculture is to reduce the usages of pesticides, bactericides, and fertilizers while improving their efficacy. Nanomaterial are being used as a nanoscale carrier for pesticide, herbicides, insecticides and disinfectants. Not to mention, some nanomaterials are being used as a delivery system for nutrients as well as, gene or DNA to plant (Rai & Ingle, 2012).

Crop loss remains a global issue causing significant economic burden to agriculture industry. It is estimated that crop losses contribute to US \$2000 billion per year (Rai & Ingle, 2012). Furthermore, it has been estimated that crop loss due to insect pest are responsible for 14% loss, plant pathogen 13% loss and weed 13% loss (Peshin & Dhawan, 2009). Additionally, it has been estimated that 30-40% of food goes to waste before consumption. It is also believed that disinfection in food packaging will help increase shelf-life. (M. A. Ali et al., 2014).

Plant disease is a major barrier to plants growth which eventually lead to crop loss. Similarly, crop loss due to infection from plant pathogens like bacteria, fungi and viruses remain global issue leading to serious economic losses. Losses are estimated to be about 40 billion dollars annually in the United States alone. Additionally, it is estimated that 20 to 40% loss in crop yield is linked to the infection caused by the plant pathogens (Fang & Ramasamy, 2015).

1.2: Antimicrobial Nanomaterials for Agriculture Purposes

In agriculture industry, livelihood of farmers is dependent on crop yield and quality. Unfortunately, plant disease caused by a wide variety of bacterial pathogens reduces yield, quality and the overall productivity. Bacterial pathogens are treated with bactericides. Cu-based biocides have been widely used for centuries, and the term contact killing has been commonly used to describe the action of copper antimicrobial agents. In fact, Cu is popularly known as broad-spectrum bactericide/fungicide in agriculture industry. Contact killing of bacteria, yeast, and viruses has been reported on metallic copper surfaces (Grass, Rensing, & Solioz, 2011). In agriculture industry, copper compounds (also known as Cu pesticides) are used as crop protectant to control bacterial and fungal disease. However, the long-term copper usage has

created some issues including the soil accumulation of copper, copper resistance development, and detrimental effects on non-target organisms (Young et al., 2017; Young et al., 2018). The excess usage of Cu pesticides has negative impact on the environmental and has been linked to water pollution. In 2017, the Environmental Protection Agency released a recommendation to reduce the copper usages and to reduce the application rate for some specific crops (Ozcan, 2019; Young et al., 2018)

In recent years, there is an increasing interest in the development of formulations with advanced Cu and copper alternatives. The purpose is to reduce Cu load per application or find a suitable alternative to Copper biocides. For instance, Magnesium (Mg) hydroxide nanoparticles (NP) with trisodium citrate or betaine coating has been demonstrated as a potential copper alternative. These particles have demonstrated growth inhibition of *X.alfalae*, *P.syringae* (plant pathogen) as well as *E.coli* after 4 hours, and significant growth reduction and killing after 24 hours. Also, Mg hydroxide NP did not cause any significant tissue injury at industry application rates as foliar bactericide when tested on tomato plant (Santra & Huang, 2020). Non-metal alternative to copper-based fungicides and bactericides has been reported also. A composite of silica and quaternary ammonia compound (fixed-quat) was tested in field conditions for controlling citrus bacterial and fungal diseases such as canker, melanose and scab. A stable fixed-quat gel (FQ-G) was produced and *in-vitro* antimicrobial studies were performed against *Xanthomonas alfalfae*, *Pseudomonas syringae*, and *Clavibacter michiganensis*. FQ-G showed good efficacy in controlling bacterial and fungal disease compared to those of several copper standards (Young et al., 2018).

Furthermore, Zinkicide ® is a zinc oxide base nanomaterial that was developed as a treatment option for Huanglongbing (HLB) a phloem-limited vascular disease in citrus. Zinkicide formulation contains ultra-small size (< 5.0 nm) ZnO nanoparticles (Naranjo et al., 2020). Zinkicide demonstrated significant antimicrobial efficacy against model pathogen when compared to conventional Cu products. Two different Zinkicide formulation (SG6 and SG4) antimicrobial properties were tested on *Xanthomonas alfalfa* subsp. *citrumelonis* and *Escherichia coli* compared to different copper formulation. Zinkicide compound exhibited exceeding or comparable efficacy when compared to commercial Copper products. Furthermore, Zinkicide TMN110 exhibited bactericidal effect on *Liberibacter crescens* while bulk-Zinc oxide works as bacteriostatic. (Graham et al., 2016; Naranjo et al., 2020; Ozcan, 2019).

Although, plant pathogens are one of the leading causes to crop loss, malnutrition is another obstacle that hinders plant growth. In agriculture, yield loss is also linked to deficiencies in micronutrients. In order to improve plant growth while reducing bacterial pathogens infection, a micronutrient-based nanoparticle with established antimicrobial activities was designed. It is noted that Copper (Cu) and Iron (Fe) are among the eight essential plant micronutrients that contribute to plant growth.

1.3: Nanomaterial Design

It is understood that there is huge demand for the developing advanced Cu or copper alternative to control plant disease while minimizing in negative environmental impact. Keeping this in mind, Fe micronutrient-based nanomaterial containing Cu is proposed in this thesis work. Nanomaterial composite of Iron Oxide (IONP) core with N-acetylcysteine Copper coating

(Cu/NAC-IONP) was synthesized, characterized and tested for antimicrobial activities. Iron oxide is extensively researched as a biocompatible magnetic material. The N-acetylcysteine (NAC) is well-known as an antioxidant supplement. NAC was used to coat Iron oxide (IO) nanoparticle to improve particles stability. Finally, Copper (II) chloride salt, a source of Cu (II) ions was added to NAC-IONP. It was hypothesized that the antimicrobial property of Cu will be retained in the Cu/NAC-IONP nanocomposite. Cu/NAC-IONP was characterized using a suite of analytical and spectroscopic techniques along with the assessment of antimicrobial properties using model bacteria.

1.3.1: Iron Oxide Nanomaterial

Iron oxide nanomaterials have gained a growing interest in scientific community for their unique superparamagnetic property and biocompatibility. For example, Iron oxide nanomaterials have been extensively investigated in biomedical research including cell labeling, tissue repair, drug delivery, Magnetic Resonance Imaging (MRI), hyperthermia treatments and immunoassays (cell tracking and tissue repair) (Cortajarena et al., 2014; Gupta & Gupta, 2005). High surface area to volume ratio of small size IONP is attractive for use as a delivery system in biomedicine and agriculture. There are three most common forms of iron oxide materials which include magnetite (Fe_3O_4), maghemite ($\gamma\text{-Fe}_2\text{O}_3$) and hematite ($\alpha\text{-Fe}_2\text{O}_3$) (A. Ali et al., 2016). Iron oxide (Fe_3O_4 and $\gamma\text{-Fe}_2\text{O}_3$) with size <10-20nm exhibit superparamagnetic properties. Likewise, maghemite and magnetite are the most commonly used iron oxide in biomedicine (Cortajarena et al., 2014).

There are many methods that are used to make Iron oxide nanomaterials including co-precipitation, thermal decomposition, hydrothermal method, solvothermal method, microemulsion method, sol-gel method, and microwave-assisted method (Song, Sun, Xiao, & Shi, 2019). Song et. al have reviewed the impact of different synthesis methods on the particle size and morphology (Song et al., 2019). Magnetic IONPs can be produced using co-precipitation of Fe^{2+} and Fe^{3+} aqueous salts using a base such as ammonium hydroxide or sodium hydroxide. In general, inorganic nanomaterials such metal oxides, hydroxides can be produced in solution state which with suitable coating can produce a stable colloidal suspension. Particles size and surface functionality can be customized by controlling synthesis parameters(Sigmund, El-Shall, Shah, & Moudgil, 2008). For example, size and shape of magnetic particles can be varied by the selection of ionic source (i.e. type of salt), pH, $\text{Fe}^{2+}/\text{Fe}^{3+}$ ratios, and coating agent. Co-precipitation is the preferred method by researcher as this method produces high quality particles with good product yield (Gupta & Gupta, 2005). It has been reported in the literature that ultra-small size Iron oxide particles in size range 2-15nm can be produced by co-precipitation method with careful adjustment of experimental parameters (Park et al., 2004). Smaller size particles due to higher surface area to volume ratio are expected to interact, absorb, and react with other atoms and molecules to achieve surface stabilization (Sigmund et al., 2008).

Iron deficiency in human is a major health problem since a significant number of people suffer from Anemia worldwide. The main source of Iron is from diet. Although iron rich fertilizer can be used to increase plants, over-fertilization could lead to free ion induced toxicity. Iron plays a key role in many enzymes that are responsible for energy transfer, nitrogen reaction,

and lignin formation. Delivery of micronutrient iron in the form of IONP is an attractive approach. Each IONP will carry thousands of Fe once delivered to the plant tissue. Particle dissolution in planta will produce both Fe^{2+} and Fe^{3+} and release in a sustained manner to fulfil the iron requirement and slow release is expected not to cause plant tissue damage (phytotoxicity).

However, there are many limitations to uncoated magnetic nanoparticles. In fact, uncoated magnetic nanoparticles are not useful for biological studies. In biological system, IONPs can form large aggregates after interaction with proteins, undergo through biodegradation and show change in magnetic property (Santra et al., 2001). With suitable coating process, IONPs (magnetite) can be stabilized in their ferromagnetic phase in biological medium (Ferrari, 2005). In general, stabilizing agent can be used to control particle aggregation to achieve stable colloidal suspension where surface charge becomes a key factor (Sigmund et al., 2008). When the shell (coating) interacts with the magnetic core, it reduced the paramagnetic properties and increase the size of the particles (Saraswathy et al., 2014). In addition, surface coating in magnetic particles must be non-toxic, biocompatible for targeted delivery (Lauren et al., 2008).

1.3.2: Copper and N-acetylcysteine Nanomaterial Coating

NAC is an antioxidant derived from amino acid L-cysteine and has many applications in medicine such as treatment for Acetaminophen overdose and mucus discharge (Mokhtari, Afsharian, Shahhoseini, Kalantar, & Moini, 2017). One study reported the use of NAC as an antimicrobial agent. NAC was shown to have a therapeutic effect on citrus plant infected with *Xylella fastidiosa* with an MIC of 6mg/ml (Muranaka et al., 2013). Additionally, NAC structure

possesses two important functional groups, carboxyl and thiol which are capable of binding with metals and metal oxides (Flora, 2009).

Copper is an essential micronutrient needed for plant growth, and it is an important element for most organism. There are over 30 types of copper containing proteins known today (Grass et al., 2011). As mentioned earlier, Cu exhibits antibacterial, antifungal, anti-inflammatory properties. These unique properties led Cu to be used in ointment, bandage and medical devices (Verma & Kumar, 2019).

Cu is a required in trace amount and it is essential cofactor for many metabolic processes. Changes to the intercellular level of copper can be detrimental to cell viability and based on this understanding one can manipulate Cu level to develop an anti-tumor formulation to induce killing of tumor cells (Verma & Kumar, 2019). Copper can also lead to cell damage and degradation of genomic and plasmid DNA (Young & Santra, 2014). Copper toxicity originates from its redox potential. Copper serves as an electron donor/ acceptor via changing in its redox state from Cu^{1+} to Cu^{2+} . Copper (Cu^{1+}) can interact with peroxide to become Cu^{2+} and produce reactive hydroxyl radicals. The redox properties of copper have been reported as the possible cause for cellular damage (Grass et al., 2011).

Killing mechanism of free copper ions is not yet fully understood. Possible cause of copper ion toxicity is that it can displace other metal ions such as iron from iron-sulfur clusters. Also, copper ion competes with other metals ions such as, zinc for protein binding site. Contact killing of Cu has been demonstrated (Grass et al., 2011). When a bacterium comes in contact with copper surface, cell membrane damage is observed followed by a leakage in the

cytoplasmic content (Grass et al., 2011). Silica gel is shown to serve as an excellent host for antimicrobial Cu. Sol-gel derived Cu-silica gel released Cu ion in solution killing bacteria while reducing toxicity to plants (Young & Santra, 2014).

Commercially available copper products (Cu oxides, Cu hydroxides, and Cu oxychlorides) are mostly hydrophobic and upon foliar application they form a film on plant surface and provide a good protection against bacterial infection. Due to low solubility of film-forming Cu, the abundance of ionic Cu is low enough not to cause phytotoxicity and sometimes enough to inhibit bacterial growth. To further improve Cu bioavailability while maintaining low phytotoxicity, a water-dispersible Cu products are needed (Young et al., 2017). Also, it is important to develop product to reduce the amount of Cu per application without compromising antimicrobial efficacy. This would require a robust material design where Cu bioavailability is maximized.

The primary purpose of this research is to prepare and characterize Cu/NAC IONP for agriculture application. It is hypothesized that Cu in Cu/NAC-IONP composite will maintain antimicrobial activity at low Cu level. This is due to the unique design of the material. Cu is captured on the surface of the IONP that provides large surface area due to small size. NAC serves as the linker connecting holding Cu on one end while anchoring with the IONP particle surface. Since Cu is exposed to the surface, its bioavailability and antimicrobial activity is not compromised. Antimicrobial activity of the Cu/NAC-IONP composite was studied against plant pathogens *Pseudomonas syringae* and animal pathogen *Escherichia coli*. *E. coli* is a gram-negative bacterium which has been most commonly used as a model system. *Pseudomonas syringae* is again a gram-negative plant pathogen. It is capable of infecting all economically

important crop species making it the most common plant pathogen. Therefore, it is one of the best studied model system for studying bacterial pathogenicity and plant-microorganism interaction (Xin, Kvitko, & He, 2018).

The characterization techniques utilized are Dynamic light scattering (DLS), Fourier transform Infrared spectroscopy (FTIR), Atomic Absorption Spectroscopy (AAS), Scanning electron microscopy (SEM-EDS), and X-ray photoelectron spectroscopy (XPS). Cu/NAC-IONP synthesized (Figure 1) through co-precipitation method. This is a micronutrient-based nanomaterial composite. It is expected that this material will exhibit antimicrobial activity against both plant and human infecting bacteria.

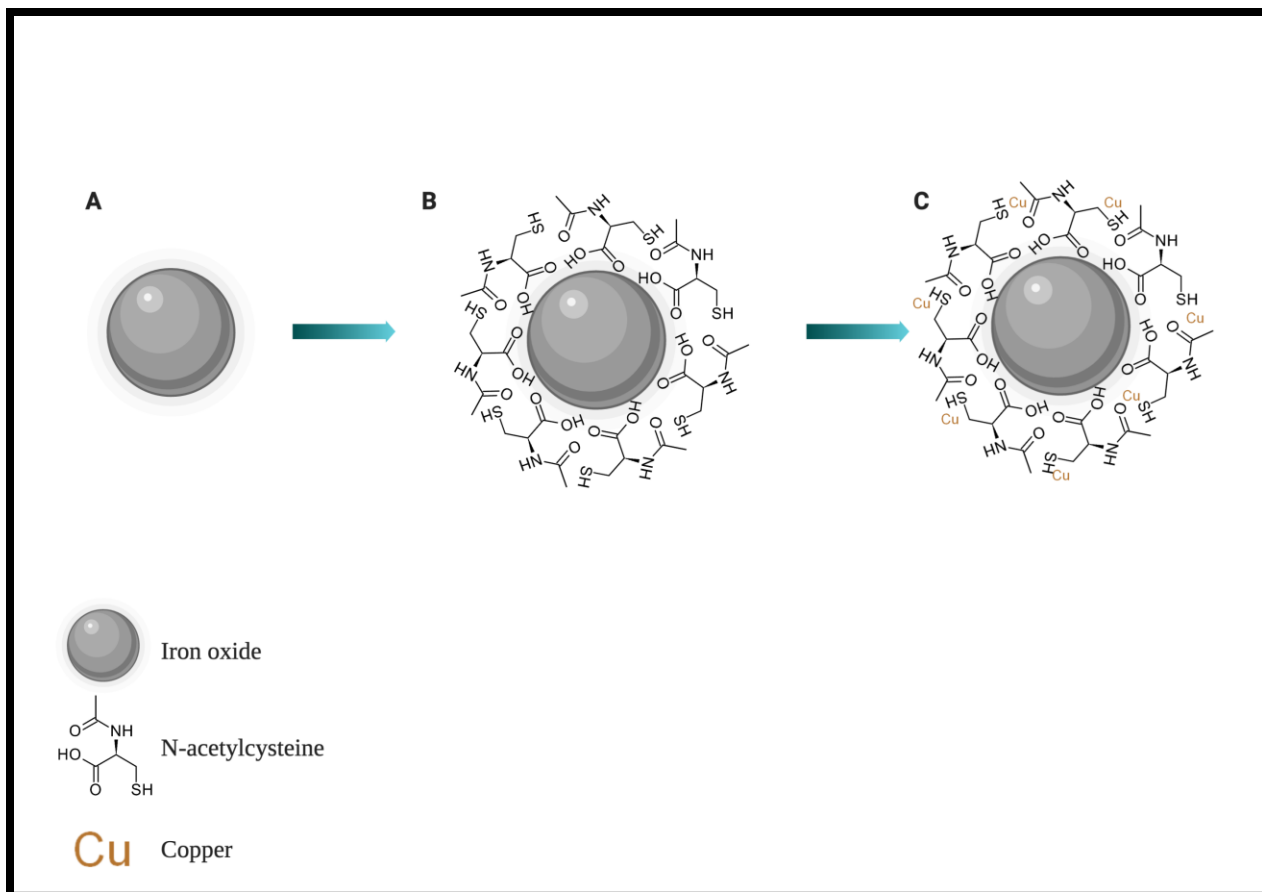


Figure 1: Nanomaterial design and possible interaction of molecules. A: Iron oxide (IONP), B: N-Acetylcysteine-Iron Oxide (NAC-IONP) and Copper/N-acetylcysteine-Iron Oxide (Cu/NAC-IONP). “Created with BioRender.com.”

CHAPTER TWO: NANOMATERIALS CHARACTERIZATION

2.1: Characterizations Techniques

Some nanomaterials exhibit unique physico-chemical, optical and electronic properties compared to their bulk material counterparts. When particle size decreases, changes can be observed in the material electronic and optical properties as well as mechanical and structural stability. Various spectroscopic and microscopic techniques are used to characterize nanomaterials. For example, electron microscopy techniques such as Scanning Electron Microscopy (SEM), Transmission Electron Microscopy (TEM) are used to characterize particle size, size distribution and surface morphology in vacuum/dry state. TEM is useful for studying crystallinity. Atomic Force Microscopy (AFM) is another technique to probe nanomaterial surface with the capabilities of measuring particle size and surface topology/roughness. X-Ray Photo Electron Spectroscopy (XPS) is used to perform surface elemental analysis and determination of metal oxidation states. X-Ray Diffraction (XRD) technique is used to determine crystallinity and also particle size. Both the XPS and XRD are run in dry state. Dynamic Light Scattering (DLS) is a light scattering based technique that measures particle size and size distribution in solution. Atomic Absorption Spectroscopy (AAS) is used to quantify the amount of metals present in a sample. Fourier Transform - Infrared Spectroscopy (FT-IR) is used to characterize nanomaterial surface coating chemistry. FT-IR spectra can suggest binding of ligand to metal surface providing information on new chemical bond formation or change in chemical bond energy. In this work, multiple techniques were utilized including AAS, DLS, FT-IR, SEM and XPS for the characterization. DLS and FT-IR facility was accessed through NanoScience

Technology Center, and AAS through the Department of Chemistry. SEM and XPS user facility was accessed through UCF Advanced Materials Processing and Analysis Center – Materials Characterization Facility.

2.1.1: Atomic Absorption Spectroscopy (AAS)

AAS is a well-established technique that can be used to detect metals and metalloid in the sample. It is a simple and reliable technique to study over 62 elements (Kalantar-zadeh & Fry, 2007). AAS analysis allow for the study of elemental composition and determine the concentration of target element in the solution. The AAS analysis uses the basic principle that free atom (plasma/gas state) absorbs specific light frequency which is characteristic. The absorbance is directly proportional to atom (metal) concentration. A standard curve is produced with known concentration of the element to determine the unknown concentration of that element present in the sample. Perkin Elmer Analyst 400 AAS (University of Central Florida, College of Sciences, Department of Chemistry) is used for this study.

AAS analysis was completed to determine Iron (Fe) and Copper (Cu) atomic concentration in the sample after purification through washing, centrifugation and drying. Atomic percentage of these element in IONP, NAC-IONP, and Cu/NAC-IONP was also calculated based on the AAS data. In addition, quantification of Cu release during the antimicrobial study was also performed using this technique. Standard solution was prepared using 1000 ppm of iron and copper (AAS standards) in 1% nitric acid. To prepare a standard curve for the analysis, eight standard samples at the following concentrations were prepared 10ppm, 5ppm, 4ppm, 3ppm, 2ppm, 1ppm, 0,5ppm, and 0.2ppm. Air and Acetylene gas were

used to fuel the flame and ionize the sample. Furthermore, the lyophilized (freeze-dried) powder of all three formulations were digested using hydrochloric acid (36-18%). Further dilutions were done as necessary.

Calculations

$$\text{Total (ppm)} = (\text{powder (mg)/hydrochloric acid (ml)}) \times 1000$$

$$\text{Fe/Cu percentage (\%)} = \text{AAS-Fe/Cu (ppm)} / \text{total (ppm)} \times 100$$

Where:

Total (ppm) is total concentration of prepared solution calculated by dividing the mass of nanomaterials by the volume of HCl times 1000.

Powder is the mass of nanomaterial synthesized used to prepare the solution.

Hydrochloric acid (HCl) is the volume of HCl added to prepare the solution.

Fe/Cu percentage (%) is the percentage of metallic Iron or Copper in the total mass of nanomaterials.

AAS-Fe/Cu (ppm) is the metallic concentration of Iron or Copper calculated from AAS analysis.

2.1.2: Dynamic Light Scattering (DLS)

DLS is popular technique that uses non-ionizing lower energy source (Red laser 633nm) to study the solution dispersibility of nanoparticles as well as, study the growth of nanoparticles in solution. DLS was used to study the hydrodynamic size of IONP, NAC-IONP, and Cu/NAC-IONP liquid samples dispersed in DI water before freeze-drying. An examination to the changes

of the particle mean diameter following the adsorption of surface molecules such as coating is expected. The instrument used is Malvern Zetasizer Nano ZS90 Light.

2.1.3: Fourier Transform Infrared Spectroscopy (FTIR)

IR spectroscopy is popular technique that utilizes IR radiation to study solid, liquid, and gases. The IR energy is enough to excite electrons to higher energy and transitions in vibration energy states which are associated with chemical bonds (Kalantar-zadeh & Fry, 2007). Each molecule has its own signature. Chemical Bonds vibrate at specific frequencies that correspond their vibrational energy (Kalantar-zadeh & Fry, 2008). This can help identify the types of bonds and functional groups in the materials IR can be used to characterize the binding of organic ligand to organic/inorganic nanomaterials surface. The FT-IR Spectrometer instrument used to study the dry powder of IONP, NAC-IONP and Cu/NAC-IONP is Shimadzu IRSpirit with QATR-S (NanoScience Technology Center). Data was graphed and edited using the equipment software and Origin software.

2.1.4: Scanning Electron Microscopy (SEM)

SEM is a powerful tool that uses a high-energy electron beam. This instrument utilizes a low-pressure vacuum system where a focused electron beam scan the surface of the sample and the generated secondary electron is used to create an image. The study was used to determine the nanomaterials morphology and size. SEM can provide 3D images with a resolution close to 20nm. Both organic and inorganic materials can be studied with SEM. The instrument used for the analysis is Zeiss ULTRA-55 FEG SEM at Materials Characterization Facility (MCF),

University of Central Florida. The freeze-dried samples were placed on top of carbon tape and loaded into the instrument. This analysis was completed with the assistance of instrument engineer Mr. Kirk Scammon.

Furthermore, SEM-EDS is a type of compositional analysis using X-Ray that helps with the mapping of the elemental distributions. It can also be used to study organic and inorganic materials. This analysis used Noran System 7 EDS with Silico Drift X-Ray Detector. Using the same samples that were imaged using electron beam for SEM were then studied using X-Ray gun for EDS analysis.

2.1.5: X-ray Photoelectron Spectroscopy (XPS)

XPS is based on the photoelectric effect. X-Ray energy can lead to photoelectron to be ejected from the first few atomic layers. In this analysis, High-vacuum system is used to study the top surface of the sample (about 10 nm). This technique helps quantify chemical and electronic state of the element. Furthermore, Peak Position corresponds to the material electronic configurations. (Kalantar-zadeh & Fry, 2008)

XPS analysis are limited to just a few Angstroms beneath the surface. The kinetic energy and number of the ejected photoelectrons is plotted as a spectrum with respect to their binding energies. The acquired spectrum is compared with spectra from known databases. A dried sample of IONP, NAC-IONP, and Cu/NAC-IONP was studied (Data shown on Supplementary Section).

CHAPTER THREE: METHODOLOGY

3.1: Nanomaterial Synthesis Procedure

Three nanomaterials formulation were prepared including Iron oxide (IONP), N-acetylcysteine-Iron Oxide (NAC-IONP), and Copper/ N-acetylcysteine-Iron oxide (Cu/NAC-IONP). All the synthesis materials were purchased from vendors with any further purification used to prepare all three formulations shown in Table 1.

Table 1: List of reagents utilized for the synthesis of nanomaterials.

<u>Materials</u>	<u>Source</u>	<u>Description</u>
Iron (III) Chloride hexahydrates, 99+%, for analysis	Acros Organics	Code:217091000 Lot: A0402423
Iron (II) chloride tetrahydrate, 99+%	Acros Organics	Code:205082500 Lot: A0390119
N-Acetyl-L-cysteine, 98+%, C ₅ H ₉ NO ₃ S	Alfa Aesar	CAS: 616-91-1 Lot: X08E074
Copper (II) Chloride, anhydrous, 99%, extra pure	Acros Organics	Code:206206530010 Lot: A0375179
Ammonia Hydroxide, ACS reagent, 28-30% solution in water, H ₅ NO	Acros Organics	CAS: 1336-21-6 Ammonia hydroxide CAS 7732-18-5 water
Hydrochloric Acid, assay (36.5-38% w/w)	Fisher Chemical	CAS 7647-01-0 Lot: 185544

3.1.1: Iron Oxide Nanoparticle (IONP) Preparation

Iron oxide was prepared utilizing co-precipitation technique adapted from (Leamy, 2003). Briefly, 0.89 mL of Hydrochloric Acid solution (HCl, 37%) in 20ml of DI water was prepared.

Then, 2.03g Ferrous Chloride Tetrahydrate ($\text{FeCl}_2 \cdot 4\text{H}_2\text{O}$) and 4.88g Ferric Chloride Hexahydrates ($\text{FeCl}_3 \cdot 6\text{H}_2\text{O}$) were dissolved in the HCl solution. In a 400ml glass beaker, 8.3ml Ammonia Hydroxide was added to 155mL of DI water ($\text{pH} > 11.5$) and began stirring using mechanical 4-bladed stirrer. The Ferrous/Ferric Chloride-HCl solution was added drop-by-drop to the stirring Ammonia Hydroxide solution and remained stirring for 30 ± 5 mins. The addition of Iron salts solution to a basic solution will lead to the precipitation of Iron salts and the formation of black Iron oxide solution. The Iron Oxide particles were washed using DI water with magnetic separation 2 times and 1 time using centrifugation (Eppendorf 5810R) at 10,000 rpm for 5 minutes. The supernatant was decanted, and the pellet was resuspended in water following sonication and vortex. The pH was then adjusted with 1% HCl solution to 6.5-7.0. The Iron Oxide solution was then centrifuged for 5 min at 10,000 rpm and freeze-dried (LabConco FreeZone 4.5 Liter Freeze Dry System Model 7750020) for 24 hours. The black powder collected was then characterized. This procedure is illustrated in Figure 2.

3.1.2: N-acetylcysteine-Iron Oxide Nanoparticle (NAC-IONP) Preparation

The preparation of N-acetylcysteine-Iron Oxide followed the preparation of IONP closely as illustrated in Figure 3. First, in a 400ml glass beaker, 8.3ml of ammonia hydroxide (28-30%) was added to 155ml of DI water, and the solution began stirring using mechanical 4-bladed stirrer. Then 2.3g of NAC was added in 20 ml of DI water. Next, the NAC solution was added to the stirring ammonia solution. The pH of the ammonia solution decreased following the addition of NAC solution. Therefore, the pH was then increased to 11.5 using the stock ammonia hydroxide solution. Next, the ferrous/ferric chloride- HCl solution was prepared as

described in Iron oxide nanoparticles preparations. Briefly, 2.03g ferrous chloride tetrahydrate ($\text{FeCl}_2 \cdot 4\text{H}_2\text{O}$) and 4.88g ferric chloride hexahydrates ($\text{FeCl}_3 \cdot 6\text{H}_2\text{O}$) were dissolved in 0.89 mL hydrochloric acid solution (HCL, 37%) in 20ml of DI water. The Iron salts solution was added drop-by drop to the stirring ammonia-NAC mixture. The pH was adjusted to 11 using stock ammonia hydroxide. The solution remained under mechanical stirring for 30 minutes \pm 5 minutes. Purification process was carried out using magnetic separation (2x) followed by dispersion with DI water and then 1x centrifugation at 10,000rpm for 5 mins. The material in the pellet was then resuspended in water following vortexing and sonication, and the pH was adjusted to 6.5-7.0 using 1% HCl. Finally, the solution was centrifuged for 5 minutes at 10,000rpm and freeze-dried for 24 hours. A black powder was obtained which was used for characterization.

3.1.3: Copper/N-acetylcysteine- Iron oxide Nanoparticle (Cu/NAC-IONP) Preparation

The procedure for the synthesis of Copper/N-acetylcysteine-Iron Oxide nanoparticles is similar to that of NAC-IONP. Figure 4 shows the step-by-step synthesis procedure. Briefly, ammonia solution was prepared by adding 8.3mL of ammonium hydroxide (28-30%) to 155mL of DI water in 400mL glass beaker. The ammonia solution was stirred using mechanical 4-bladed stirrer. Next, NAC solution was prepared by adding 2.3g N-Acetyl-L-cysteine in 20 ml of DI water. After that, the NAC solution was added to the stirring ammonia solution. The NAC/ammonia solution pH adjusted to 11.5 using Ammonia Hydroxide (28-30%). The Ferrous/Ferric chloride- HCl solution was prepared the same as described in the previous two sections. The Iron salts solution was added drop-by drop to the stirring ammonia/NAC solution. After 30 minutes stirring, copper chloride solution was prepared by adding 3.93g of anhydrous

copper (II) chloride to 20 ml of DI water. The copper chloride solution was then added to the NAC-Iron Oxide. The pH was readjusted to 12 using ammonium hydroxide (28-30%) and stirring continued for 30 minutes \pm 5 minutes. To remove any excess unbound chemicals, the product was purified. The process involved 2x magnetic separation followed by re-dispersion of the pallet and then 1x centrifugation at 10,000rpm for 5min. The pallet was then resuspended in DI water and the pH was adjusted to 6.5-7 using 1% HCl. Finally, the solution was centrifuged for 5min at 10,000rpm and freeze-dried for 24 hours. The product in the dry state appeared as brown-black powder which was then used for characterization.

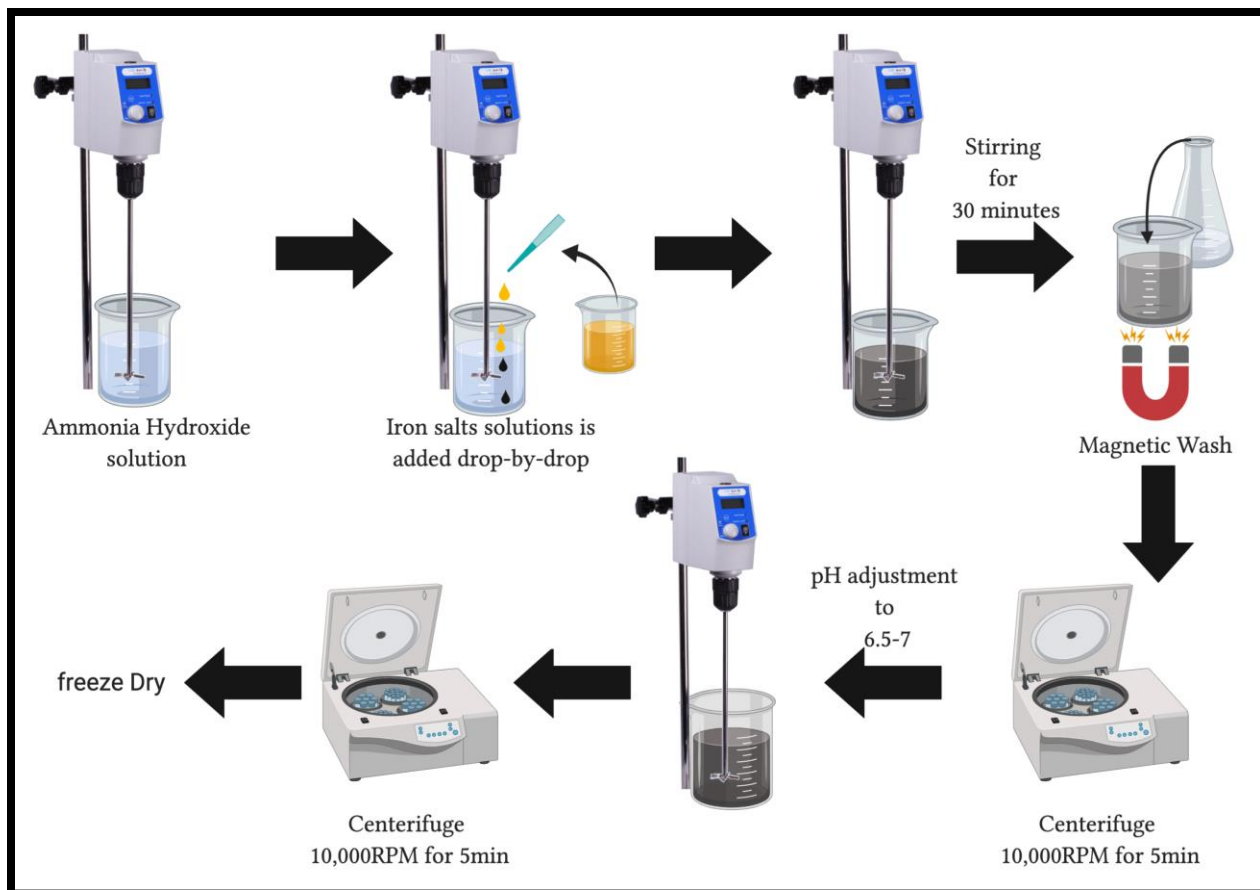


Figure 2: A simplified illustration of the synthesis procedure completed to produce IONP. “Created with BioRender.com.”

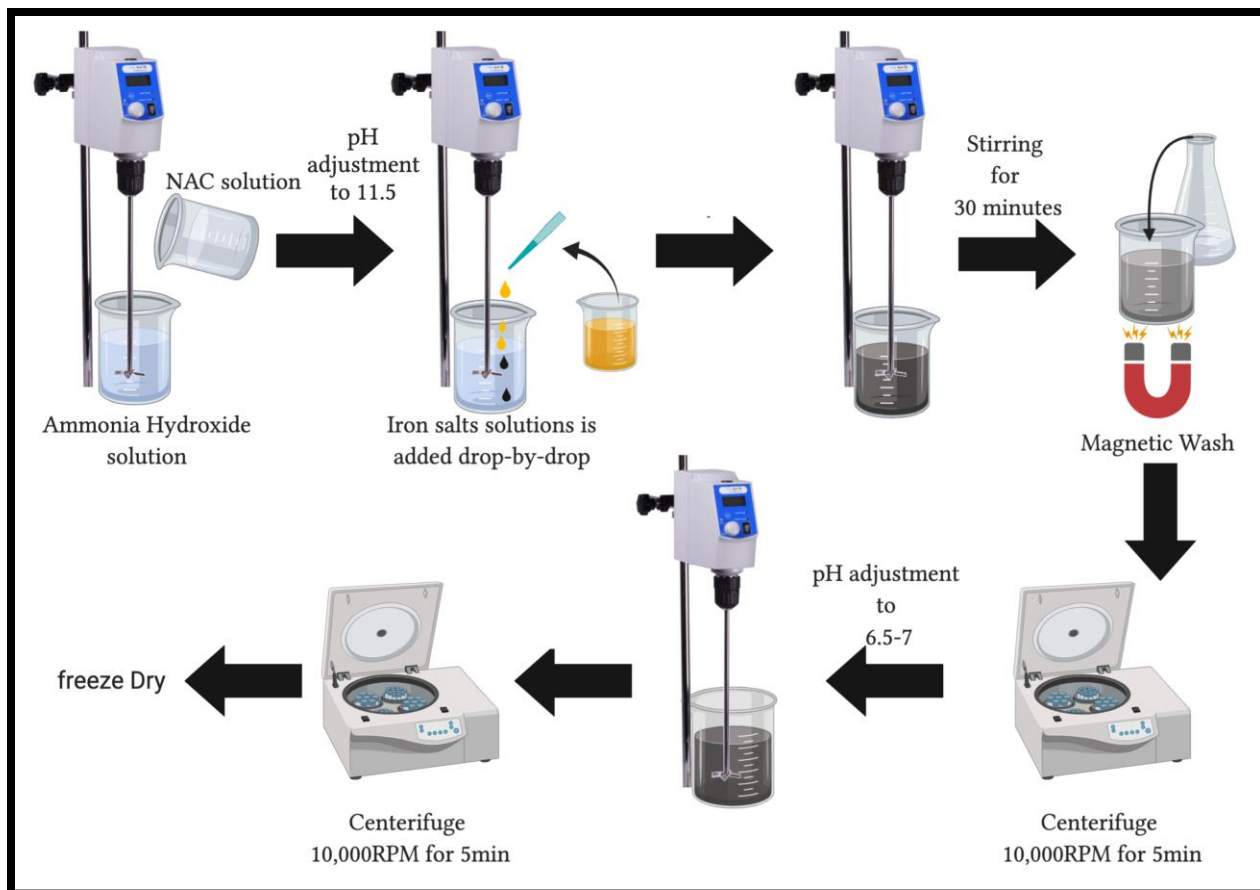


Figure 3: A simplified visual illustration of the synthesis procedure taken to produce NAC-IONP. “Created with BioRender.com.”

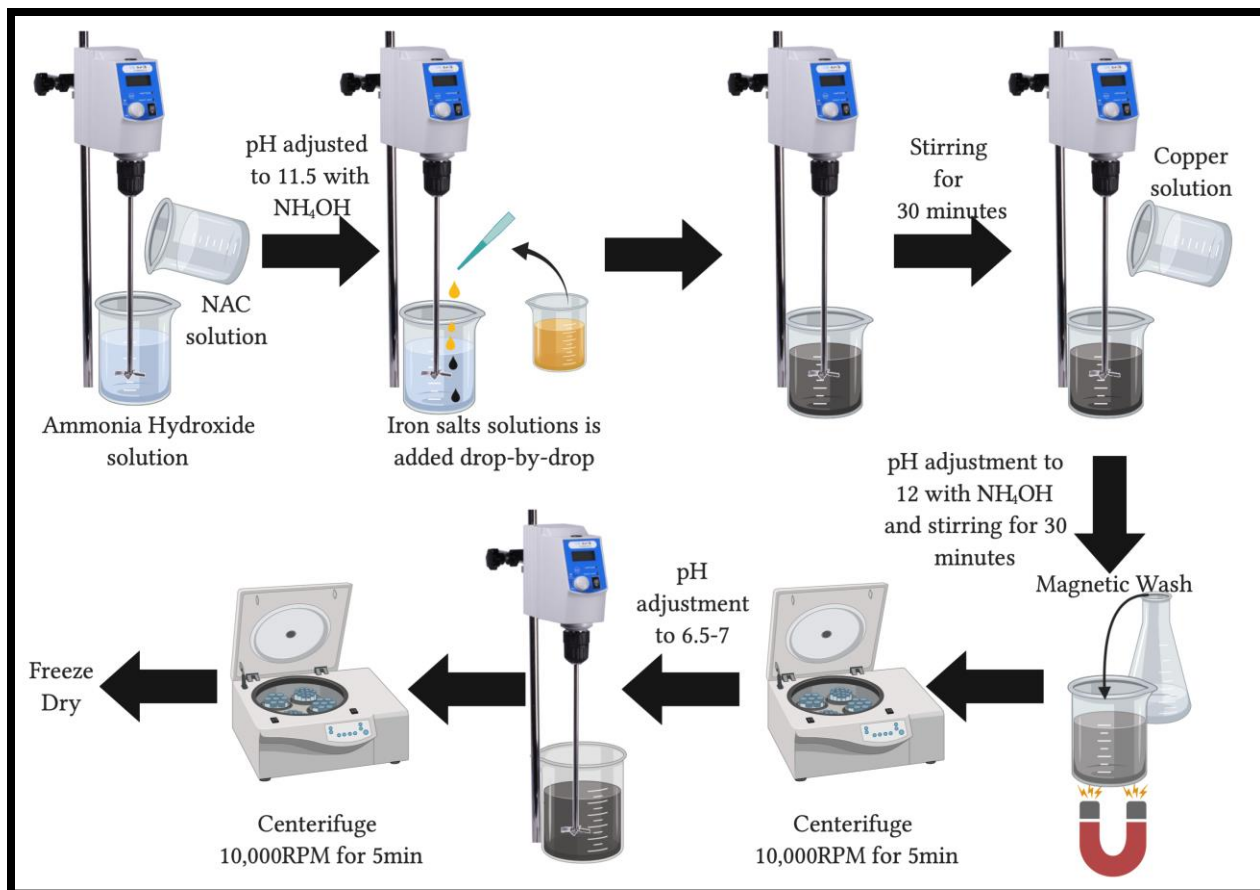


Figure 4: A simplified illustration of the synthesis procedure of Cu/NAC-IONP “Created with BioRender.com.”

3.2: Antimicrobial Studies

3.2.1: Determination of Antimicrobial Activity of Nanomaterials

The IONP, NAC-IONP and Cu/NAC-IONP were characterized in the powder form as they exhibit limited water solubility. A standard protocol developed by the American Society for Testing and Materials (ASTM) was used to study the antimicrobial activity of NAC-IONP and Cu/NAC-IONP powder. ASTM E2149 titled “Determining the Antimicrobial Activity of Immobilized Antimicrobial Agents Under Dynamic Conditions” method was adapted with some

modification (E2149–13a, 2013) as shown in Figure 5, the antimicrobial activity of Cu/NAC-IONP and NAC-IONP was tested against two model system *Escherichia coli* for Animal infecting bacteria and *Pseudomonas syringea* for plant infecting bacteria.

3.2.1.A: Antimicrobial Activity of NAC-IONP and Cu/NAC-IONP on *Escherichia coli*

To prepare liquid culture and serial dilutions for plating was completed following the a published Protocol (Wiegand, Hilpert, & Hancock, 2008) with some modifications. To prepare *E.coli* culture for antimicrobial testing, a loop full of frozen *E.coli* stock was streaked on a LB agar plate and incubated at 37⁰C. After 18-24 hours, 4-5 colonies are used to prepare the liquid culture. The optical density of the liquid culture was recorded and 10⁸ CFU ml⁻¹ suspensions was prepared done using LB broth. To investigate bacteria percent reduction after adding the nanomaterials ASTM E2149 protocol was followed. Next, to prepare 10⁶ CFU ml⁻¹ standard bacterial culture for testing in three 50ml sterile centrifuge tubes 50ml of LB broth and 500ul of 10⁸ bacterial culture was transferred to each tube. The three tubes were labeled as no treatment (control), NAC-IONP, and Cu/NAC-IONP respectively. 1.0 gram each of NAC-IONP and Cu/NAC-IONP was added to their labeled tube. The tubes were incubated at 37⁰C in a tube rotator. Samples from all treatment tubes were plated following standard serial dilution plating at different time points. The plates were then incubated at 37⁰C for 24hr before recording colony count and calculating CFU/ml and percent reduction.

3.2.1.B: Antimicrobial Activity of NAC-IONP and Cu/NAC-IONP on *Pseudomonas syringea*

The same steps taken to examine the antimicrobial activity of NAC-IONP and Cu/NAC-IONP on *E.coli* were completed for *Pseudomonas syringea*. Some modification to incubation temperature and durations were done. In summary, ASTM E2149 protocol have been modified to examine the antimicrobial activity of the materials against plant pathogen model bacteria *P. syringae*. First, *P. syringae* frozen stock was streaked on NA plate and incubated at 28⁰C. After 36-48 hours, 4-5 colonies are used to prepare 10⁸ CFU ml⁻¹ bacterial suspensions and the cell density is confirmed by OD at 600nm absorbance. Then, 10⁸ CFU/ml diluted to 10⁶ CFU ml⁻¹ using nutrient broth. Three 50 ml centrifuge tubes were labeled with blank (no treatment), NAC-IONP, and Cu/NAC-IONP, 50 ml of 10⁶ CFU ml⁻¹ is added and 1.0 gram of each nanomaterial is added to respectable tubes. The tubes were incubated at 28⁰C in a tube rotator. Samples from all treatment tubes were plated following standard serial dilution plating at different time points. The plates were then incubated at 28⁰C for 24hr before recording colony count and calculating CFU/ml and percent reduction.

Percent Reduction Calculation

To determine antimicrobial activity of NAC-IONP and Cu/NAC-IONP

Log₁₀ Bacteria Reduction= Log₁₀ (B)- Log₁₀(A)

$$\text{Reduction, \% (CFU/mL)} = \frac{B-A}{B} \times 100$$

A= is the CFU/mL of the treated substrate after specific contact time

B= is the CFU/mL of the inoculum only after specific contact time

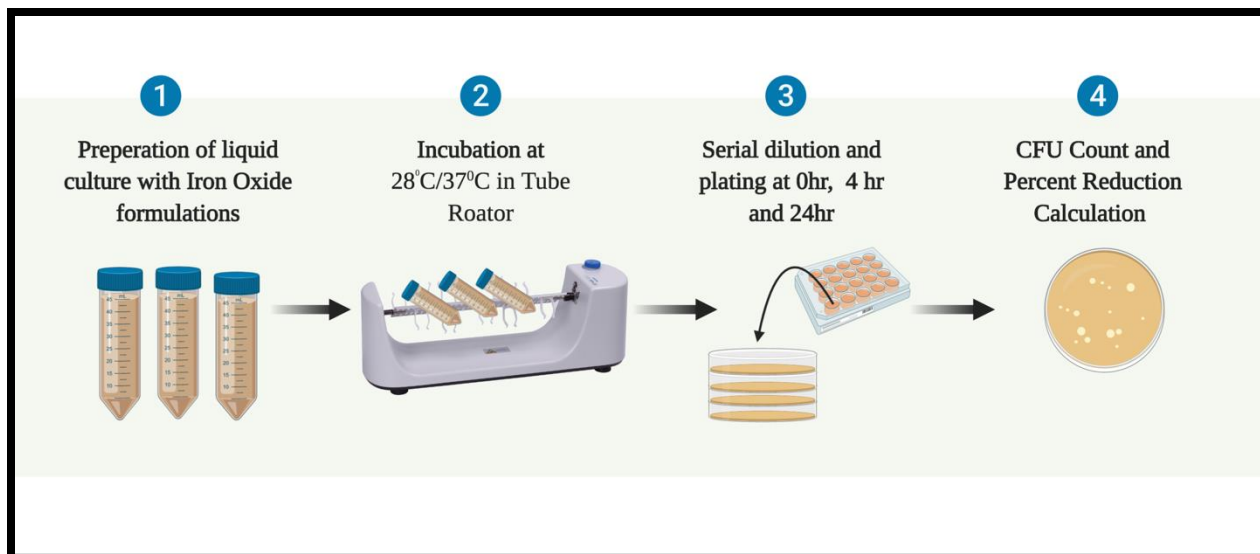


Figure 5:A simplified illustration of the steps taken to investigate the antimicrobial activity of NAC-IONP and Cu/NAC-IONP “Created with BioRender.com.”

3.2.2: Quantification of Copper Release

Copper release in the media following 24-hour incubation was calculated using the Atomic Absorption Spectroscopy. This experiment is a continuation of the procedural steps taken for the determination of antimicrobial activity of powder nanomaterial products. As shown in Figure 6, three 50ml centrifuged tubes labeled as no treatment (Blank), NAC-IONP, and Cu/NAC-IONP, and 1.0 gram of each NAC-IONP and Cu/NAC-IONP is added to respectable tubes. Next, 50ml of 10^6 CFU ml^{-1} bacteria culture is added to all three tubes. For *E.coli* bacteria culture tubes were incubated at 37°C in tube rotator. After 24 hours, the tubes were placed on a magnet to separate the iron oxide nanomaterials from supernatants containing free ions. Furthermore, 5.0 mL of each tube were digested using 5.0mL of hydrochloric acid (36.5-38%). Finally, Iron and Copper concentration is determined using Atomic Absorption Spectroscopy.

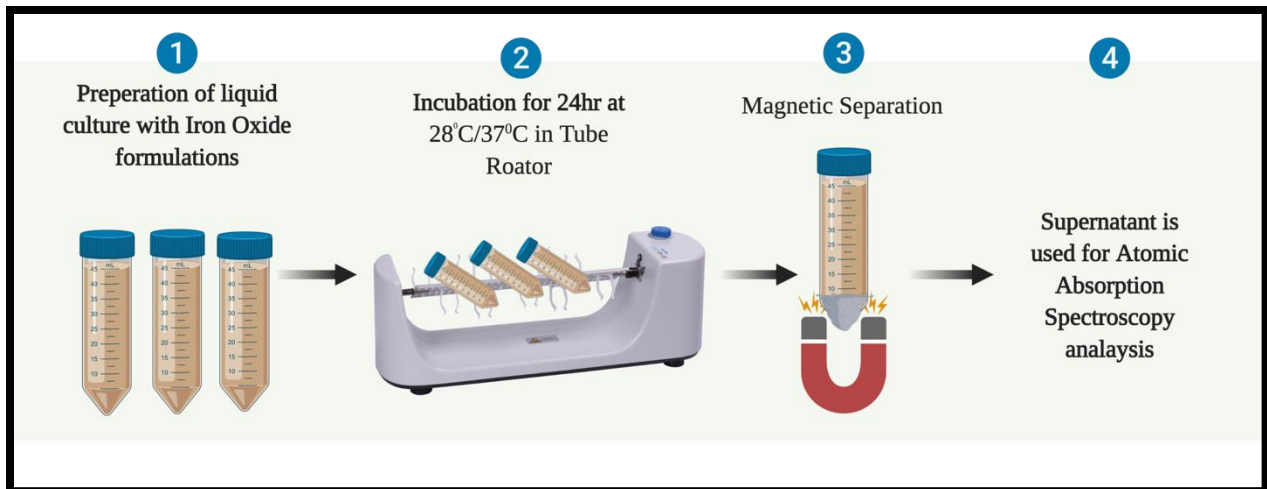


Figure 6: An illustration of procedure taken to calculate copper release in the media following 24-hour incubation. “Created with BioRender.com.”

CHAPTER FOUR: RESULTS & DISCUSSION

The optimized synthesis protocols for IONP, NAC-IONP and Cu/NAC-IONP are shown in Figures 2-4. Iron Oxide nanoparticle core was synthesized using co-precipitation method at high pH. This is an example of bottom-up nanomaterials synthesis approach. Co-precipitation is one of the most popular procedures when it comes to Iron Oxide nanoparticles synthesis in aqueous phase. The key steps are the optimization of Iron salts concentration, the strength of the base, mechanical stirring time and the pH of the reaction mixture. This synthesis process is suitable for large scale production for future agricultural applications. The NAC has multiple role. It is a biocompatible antioxidant molecule which is used as food supplement. It is an excellent nanoparticle surface coating agent that minimizes the growth of the primary particle. It serves as a bidentate ligand coupling Cu with the IONP magnetic core. A series of nanomaterials characterizations techniques have been used to further study the nanomaterial structure, composition and properties.

During the synthesis protocol optimization process, several troubleshooting steps were carried out. Poor quality (brown color, non-magnetic) IONP is produced if the reaction is carried out in a beaker or bucket larger than 400ml size (with a large opening). Also, mechanical stirring speed must be controlled to prevent bubble formation. Formation of bubble in the reaction mixture results in poor quality IONP. For the synthesis of NAC-IONP, it is essential to add NAC to the ammonia solution first prior to adding the solution containing iron salts. The alternative procedure (i.e. post coating of IONP with NAC) resulted IONP which after purification did not show any FTIR peaks characteristic to NAC. Also, stirring time is important for the synthesis of

NAC-IONP and Cu/NAC-IONP. It was determined that minimum of 30 minutes mechanical stirring is needed for the NAC coating and Cu immobilization.

A series of techniques were used to characterize the nanomaterials. AAS was used to quantify the concentration of metals Iron (Fe) and Copper (Cu) in the nanomaterials. AAS analysis is a common technique that allows for the estimation of metal concentration in the sample. Others have used AAS analysis to determine the iron content in composite materials (Huang, Shieh, Shih, & Twu, 2010). As shown in Table 2, the total iron weight percentage (Fe %) was estimated to be 17.8 ± 0.8 in IONP, 18.3 ± 4.3 in NAC-IONP, and 17.7 ± 2.6 in Cu/NAC-IONP. Furthermore, the total copper weight percentage (Cu %) was calculated to be 0.9 ± 0.3 in Cu/NAC-IONP.

Table 2: Atomic Absorption Spectroscopy Analysis and the calculations of weight percentage (Wt%) of total Iron and total Copper in each synthesized nanomaterial including Iron Oxide, NAC-Iron Oxide, and Copper/NAC-Iron Oxide.

Nanomaterials	Fe (%)	Cu (%)
<u>NAC-IONP</u>	18.3 ± 4.3	----
<u>Cu/NAC-IONP</u>	17.7 ± 2.6	0.9 ± 0.3

Dynamic Light Scattering study was completed to estimate hydrodynamic size of the materials. Figure 7, 8, and 9 display DLS results with average particle size and size distribution of IONP, NAC-IONP, and Cu/NAC-IONP, respectively. DLS data show that IONP size ranges from 59 to 712 nm and the average diameter (the highest number %) is estimated to be 91 nm. NAC-IONP shows bimodal particle size distribution in the range between 141.8-458.7nm and 955.4-2669nm with average diameter of 220nm. The large Z-average value (Table 3) and

bimodal size distribution suggest that NAC-IONPs are aggregated. Particle size distribution of Cu/NAC-IONP is in the range between 396 nm and 1718 nm with average diameter of 712 nm. The increase in the overall hydrodynamic size suggest that copper and NAC adsorption on the surface has led to increase in the overall diameter of the materials. DLS data of all three materials were compiled in Figure 10. DLS data suggest NAC binding to IONP and also Cu binding to IONP-NAC. Table 3 compiles DLS data showing the Z-average, polydispersity index and count rate along with the pH of the solution. The wider particles size distribution and large Z-average (Table 3) suggest that particles aggregate with time. Z-average appears to be the highest for NAC-IONP this could be due to the formation of disulfide bond between the thiol group in NAC which is prevented when some of these group are bound with copper.

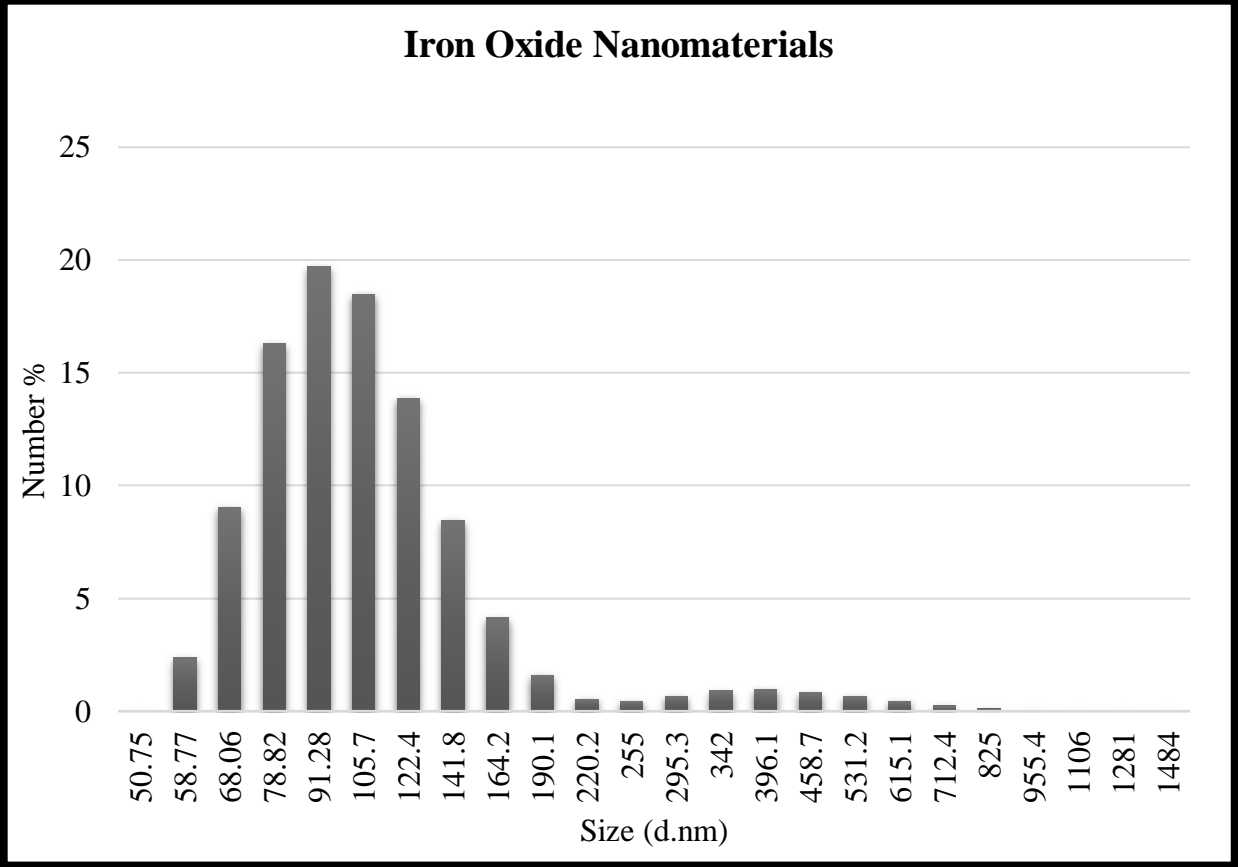


Figure 7: DLS analysis of Iron Oxide nanomaterials before freeze drying.

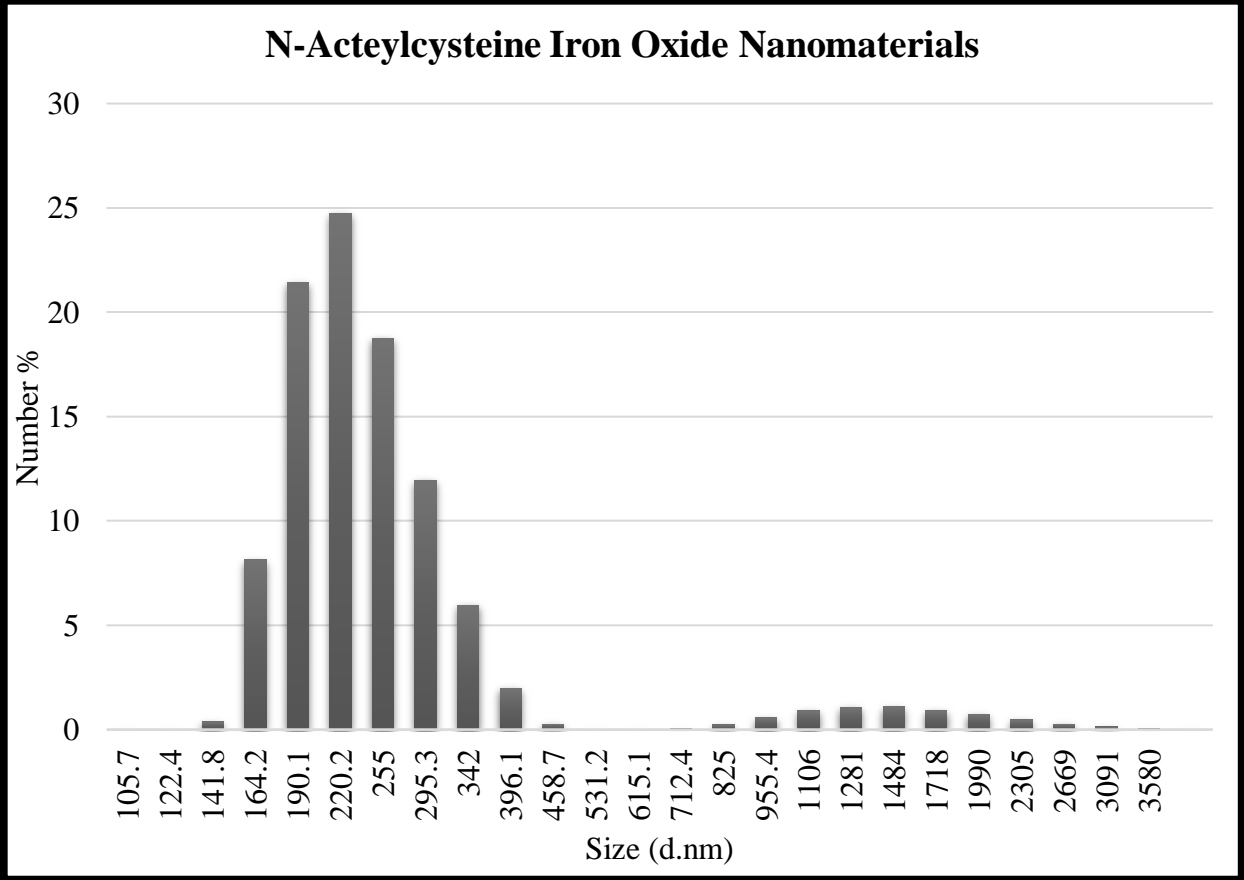


Figure 8: DLS analysis of NAC-Iron Oxide before freeze drying.

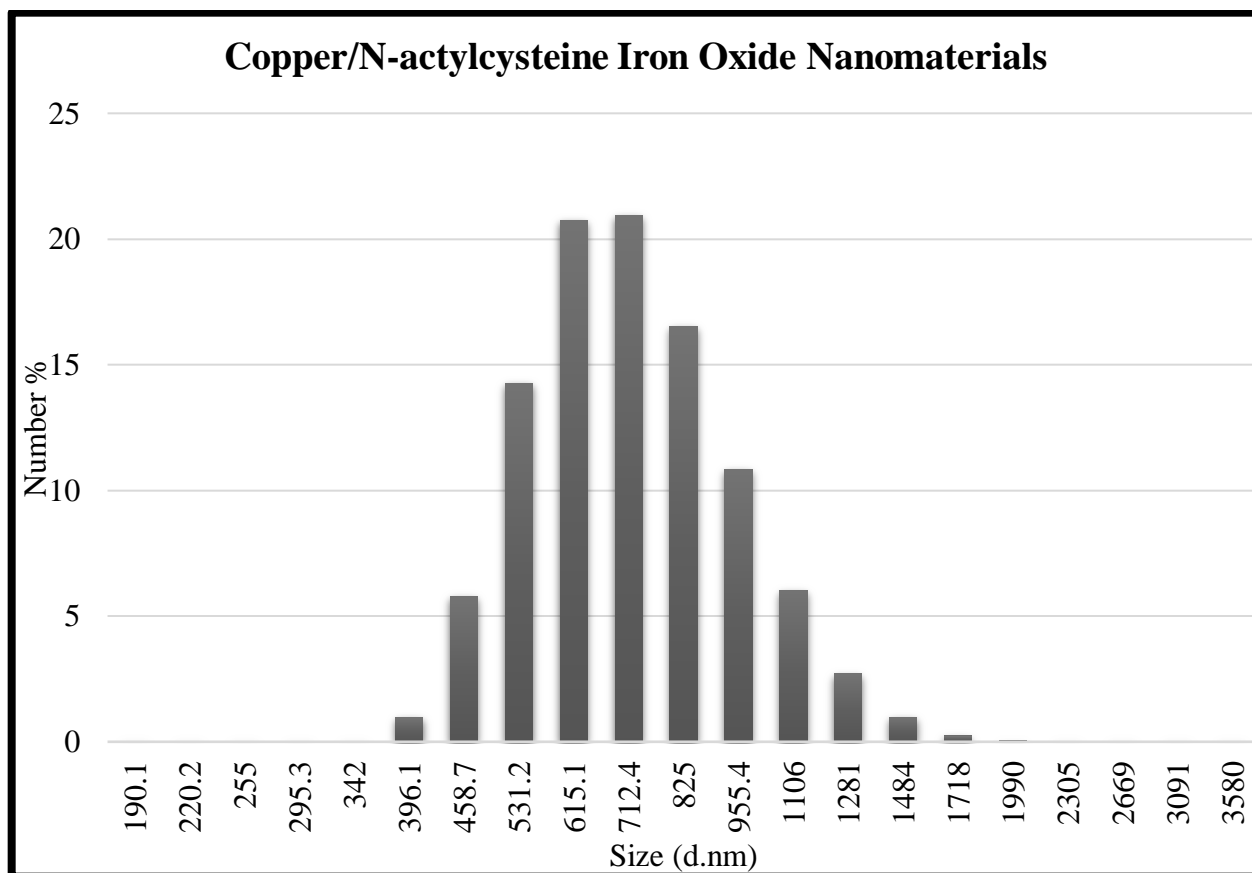


Figure 9: DLS analysis of Cu/NAC-Iron Oxide before freeze drying.

Table 3: Summary of DLS analysis including the Z-Average, Polydispersity Index (PDI), count rate and pH of the three synthesized nanomaterials Iron oxide, NAC-Iron Oxide, and Cu/NAC-Iron oxide

	<u>IONP</u>	<u>NAC-IONP</u>	<u>Cu/NAC-IONP</u>
Z-Average	547.4	1282.3	864.2
PDI	0.544	0.546	0.258
Count Rate	141.2	138.0	185.5
pH	8.97	7.93	7.81

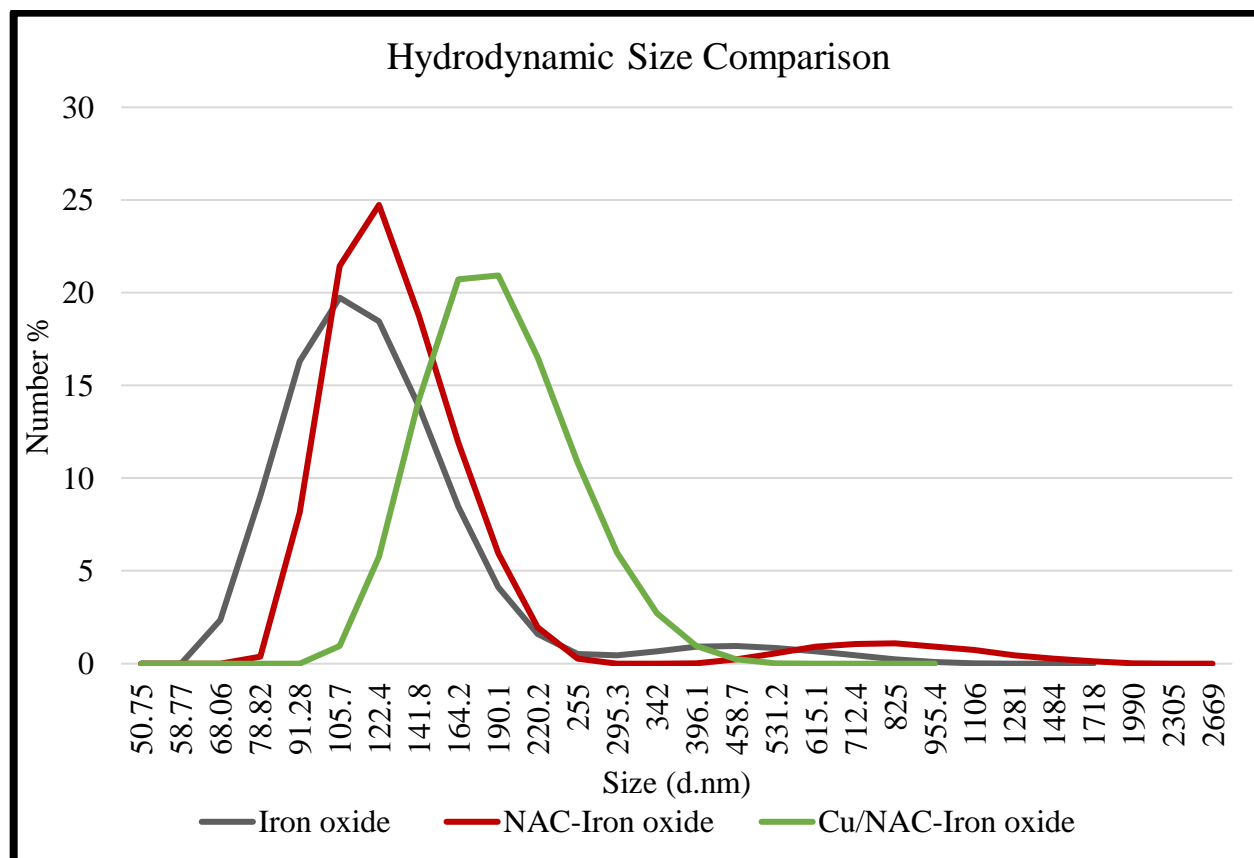


Figure 10: Hydrodynamic size comparison between Iron oxide, NAC-iron oxide, and Cu/NAC-Iron Oxide.

Moreover, FTIR was used to characterize chemical bonds present in the composite nanomaterials. Changes to their chemical structure lead to IR signature such as, peak shift, peak disappearance or appearance of new peaks. In this study, the lyophilized powder was used for the FT-IR study. FTIR spectrum of IONP shows a peak at 540 cm^{-1} which is assigned to Fe-O bond stretching frequency (Figure 11). Table 4 summarizes other FT-IR peaks located at 400 cm^{-1} and 570 cm^{-1} which are assigned to Fe-O bond in magnetite (Fe_3O_4) (Namduri & Nasrazadani, 2008).

FT-IR peaks located at 579 cm^{-1} and 593 cm^{-1} were assigned to iron oxide (Fe (II) and Fe(III)) Fe-O bond for octahedral and tetrahedral sites (Huang et al., 2010).

The NAC-IONP FTIR spectrum (Figure 12) shows a series of peaks which have been assigned to key bonds present in both N-acetylcysteine and Iron Oxide. Peak at 565 cm^{-1} and 890 cm^{-1} are assigned to Fe-O and α - FeOOH vibration, respectively. Table 5 summarizes other FT-IR peaks which match with the literature data published by other groups. For instance, others authors have labeled α - FeOOH Goethite (OH stretch) 890 cm^{-1} and 810 cm^{-1} (Namduri & Nasrazadani, 2008). Also, peaks at 796 cm^{-1} and 2975 cm^{-1} are assigned for different vibrational mode of C-H bond, while 1382 cm^{-1} is for absorption band of -COOM. Others authors have labeled -COOM peaks at 1388 cm^{-1} (Sun, Yang, Cui, & Liu, 2014). Additional peaks were assigned at 1051 cm^{-1} and 1096 cm^{-1} to C-O. In addition, 1634 cm^{-1} peak was assigned to H-bonded carbonyl group. FTIR spectroscopy studies of NAC have shown that H-bonded carbonyl stretching appear in the range between $1620\text{-}1660\text{ cm}^{-1}$. The FT-IR broad peak located at 3141 cm^{-1} is assigned to O-H group (Sun et al., 2014).

Lastly, Figure 13 displays the FTIR spectrum of Cu/NAC-IONP. Although, Cu/NAC-IONP and NAC-IONP share about the same assigned peaks, some minor spectral shift is observed as recorded in Table 5. Briefly, a peak at 574 cm^{-1} and 891 cm^{-1} was assigned to Fe-O and α - FeOOH vibration, respectively. Different vibrational mode of C-H is assigned for peaks at 798 cm^{-1} and 2975 cm^{-1} , and 1384 cm^{-1} is labeled as -COOM; while two C-O peaks are assigned at 1050 cm^{-1} and 1094 cm^{-1} . O-H peaks is broad and found at 3175 cm^{-1} . Finally, 1634 cm^{-1} was labeled for H-bonded carbonyl. There are no significant changes in the FTIR spectra of

NAC-IONP and Cu/NAC-IONP probably due to copper is binding to NAC through ionic interactions

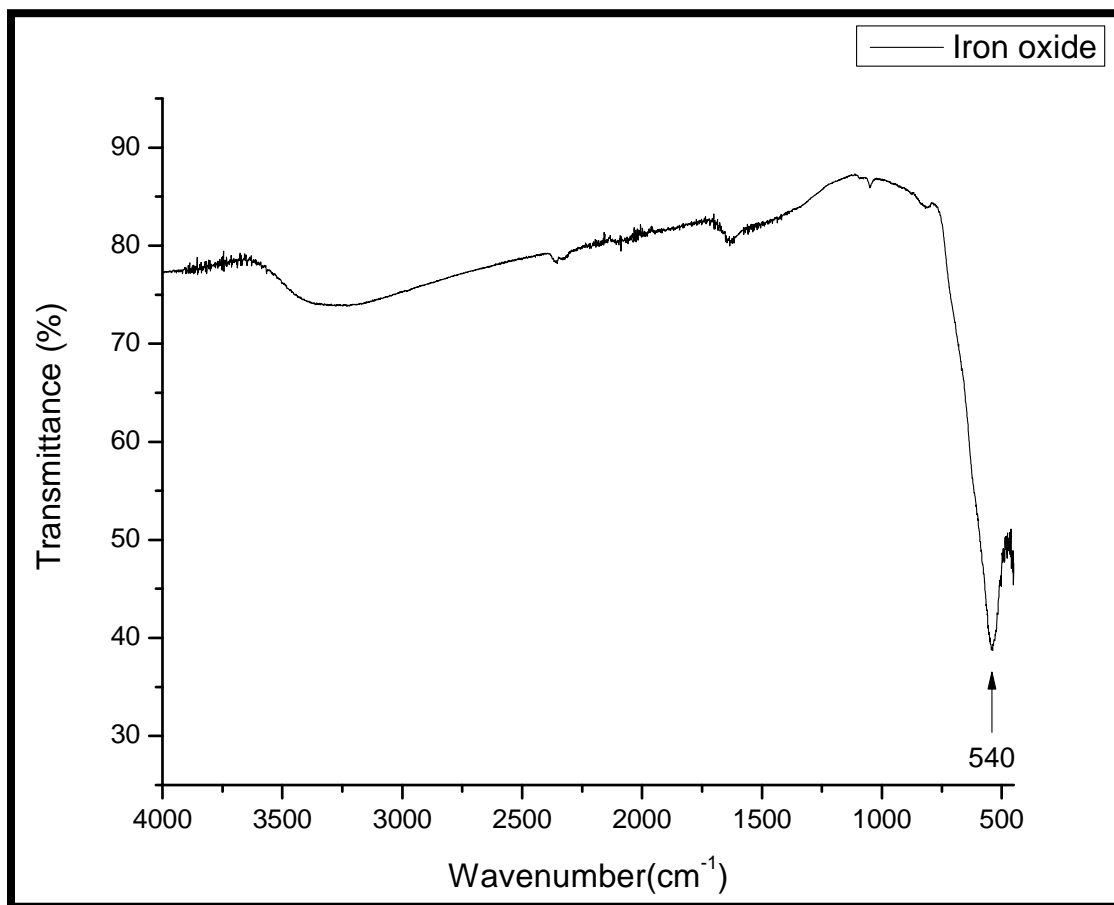


Figure 11: FTIR spectrum of Iron Oxide nanomaterial.

Table 4: Iron Oxide FTIR assigned peaks and their recognized chemical and previously identified similar peaks in the literature.

Chemical Bonds	Previously Identified Wavenumber (cm⁻¹)	Assigned Wavenumber (cm⁻¹)
Fe-O	Fe-O (magnetite) 570, 400 (4)	540

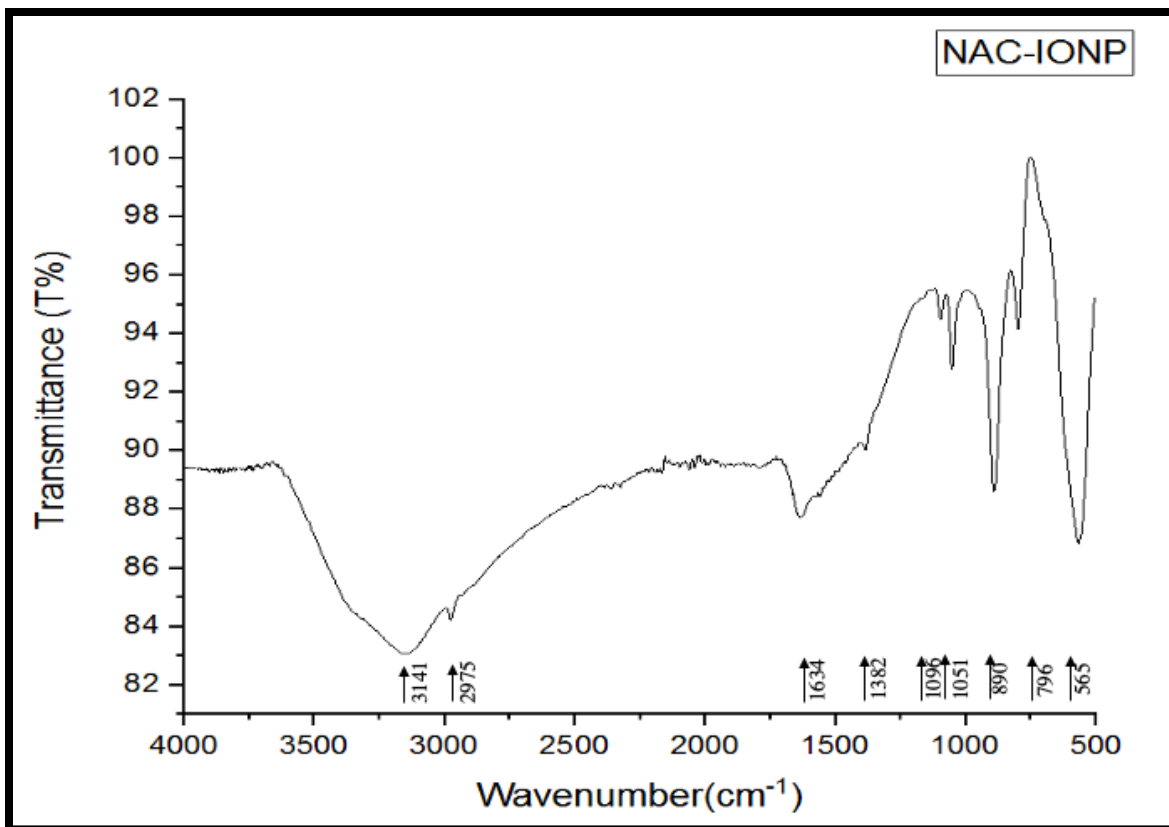


Figure 12: FTIR spectrum of NAC-Iron Oxide.

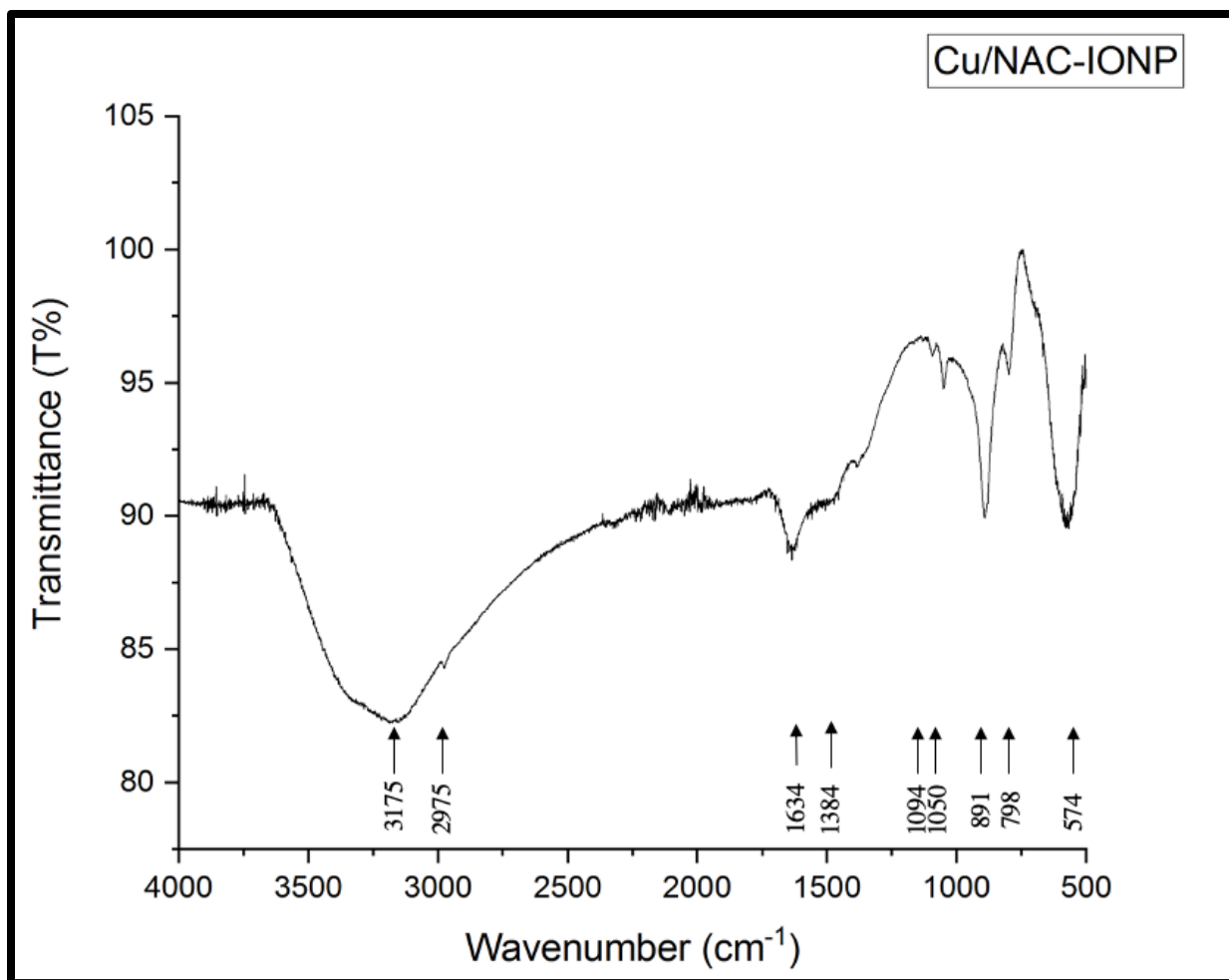


Figure 13: FTIR spectrum of Cu/NAC-Iron Oxide nanomaterial.

Table 5: FTIR assigned peaks, their recognized chemical bond and previously identified peaks in the literature for NAC-IONP and Cu/NAC-IONP.

<u>Chemical Bonds</u>	<u>Previously Identified Wavenumber (cm⁻¹)</u>	<u>NAC-IONP Assigned Wavenumber (cm⁻¹)</u>	<u>Cu/NAC-IONP Assigned Wavenumber (cm⁻¹)</u>
Fe-O	(magnetite) 570, 400	565	574
C-H	C-H bending (780 ± 20)	796	798
α- FeOOH	Goethite (OH stretch) 890 and 810	890	891
C-O	Alcohol/C-O stretching (1124-1087), (1085-1050)	1051, 1096	1050, 1094
-COOM	1385-1380	1382	1384
H-bonded carbonyl	1620-1660	1634	1634
C-H	C-H stretch/ alkane (3000-2840)	2975	2975
O-H	O-H stretch (3200-2700)	3141	3175

Scanning electron microscopy (SEM) was used to estimate particle size and image surface morphology. SEM image of IONP powder is shown in Figure 14. Image shows the appearance of spherical particles which are aggregated. The average IONP particles size was estimated to be about 18 nm using ImageJ software. The SEM particle morphology appears to be similar to what is reported elsewhere (Prodan et al., 2013). Additional SEM images of Iron oxide powder at lower magnification are provided in the supplementary information. The SEM images of NAC-IONP are shown in Figure 15 and Figure 16. Particles appear to be highly aggregated even though primary particle size was comparable to IONPs. A crude estimation of particle size was done based on ImageJ, showing average size to be 13 nm. Figure 17 shows SEM images of Cu/NAC-Iron Oxide at 20KX magnification. Cu/NAC-IONP again appeared to be highly

aggregated. SEM surface morphology of NAC-IONP and Cu/NAC-IONP appear to be quite similar. Similar observation was made by others for the NAC functionalized Fe_3O_4 magnetic core coated with silver nanoparticles (Huang et al., 2010). It is noticed that SEM particle size and size distribution results complement with the DLS data in solution state, both showing particle aggregation.

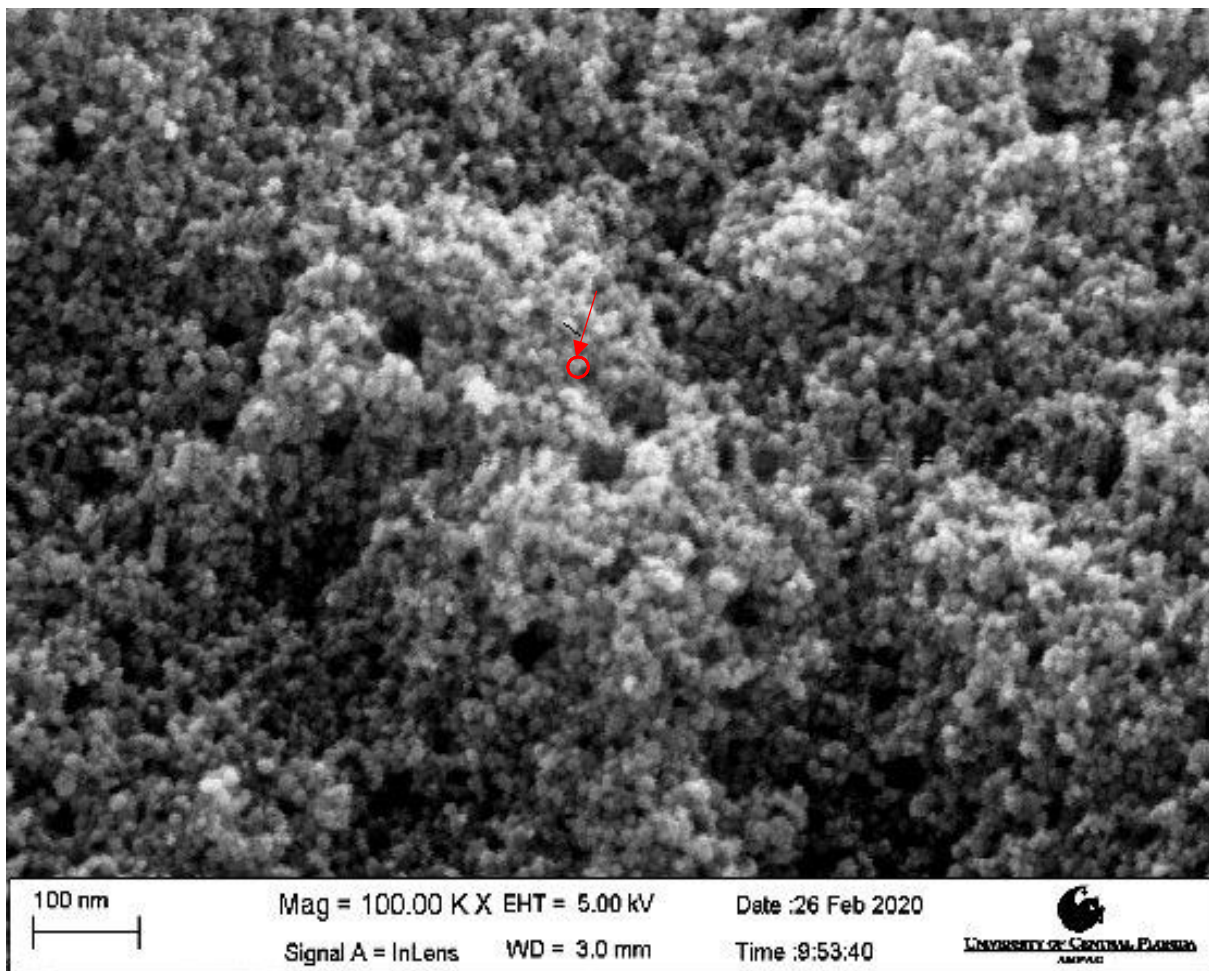


Figure 14: SEM images of Iron Oxide nanoparticle.

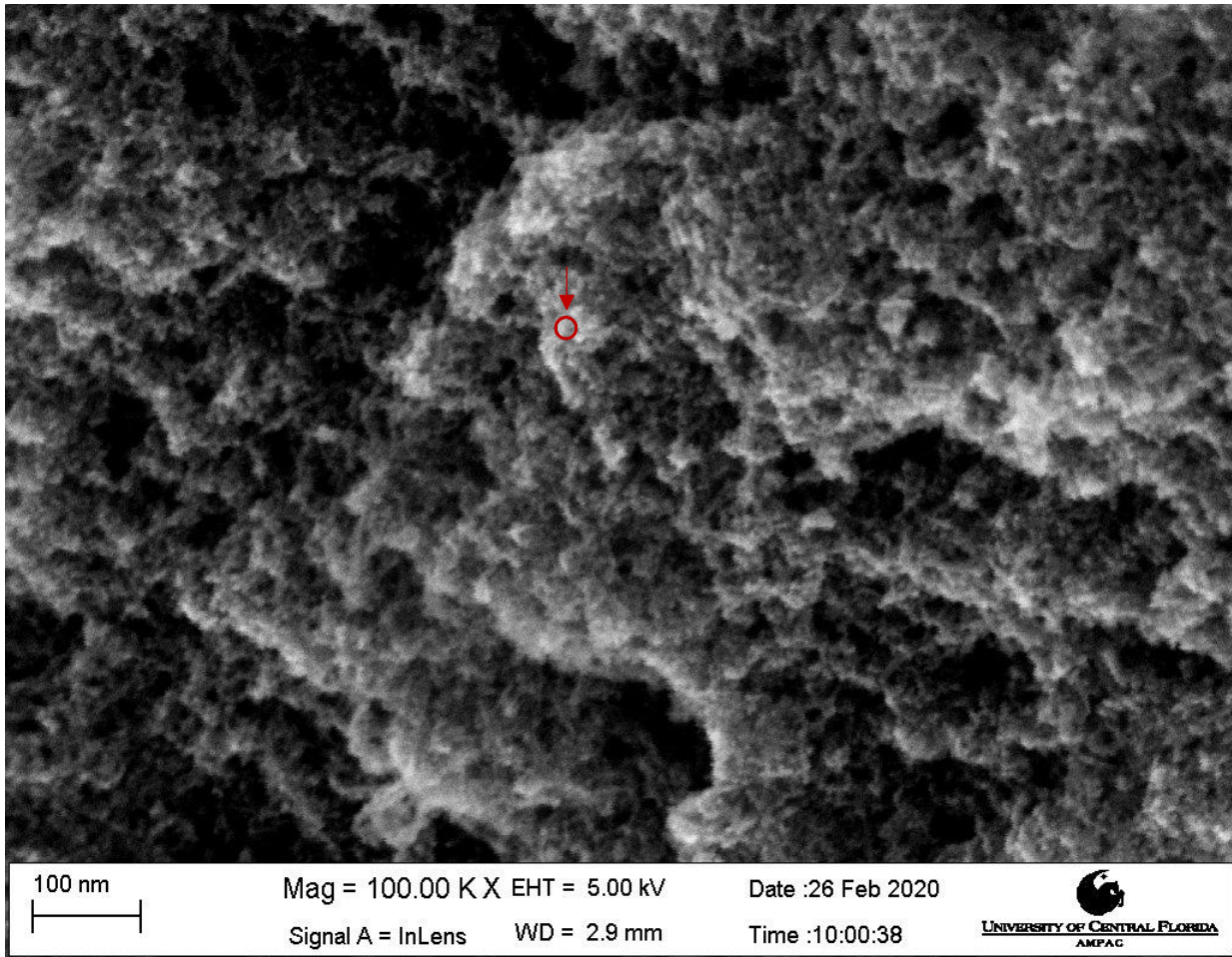


Figure 15: SEM Images of NAC-Iron Oxide.

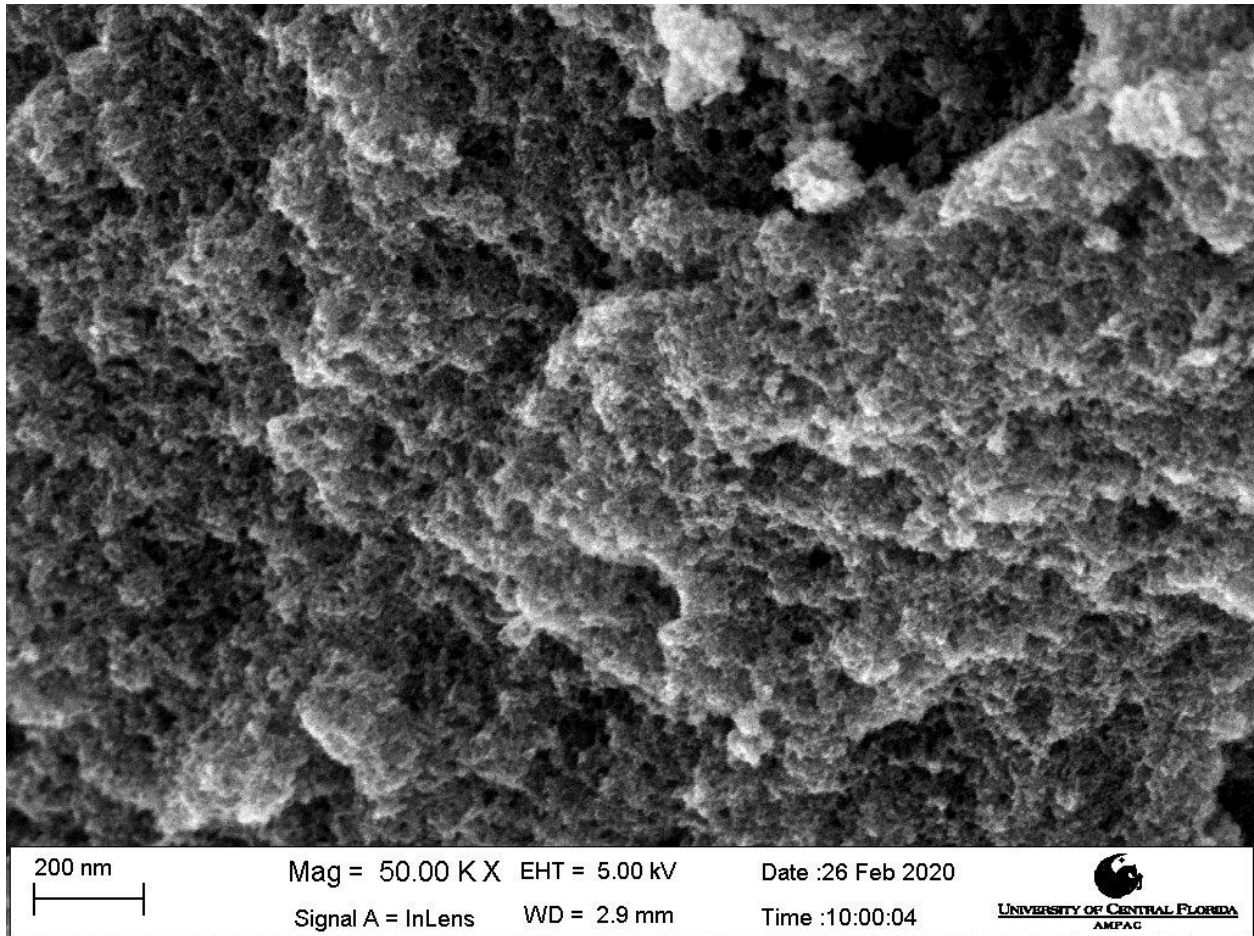


Figure 16: SEM Images of NAC-Iron Oxide.

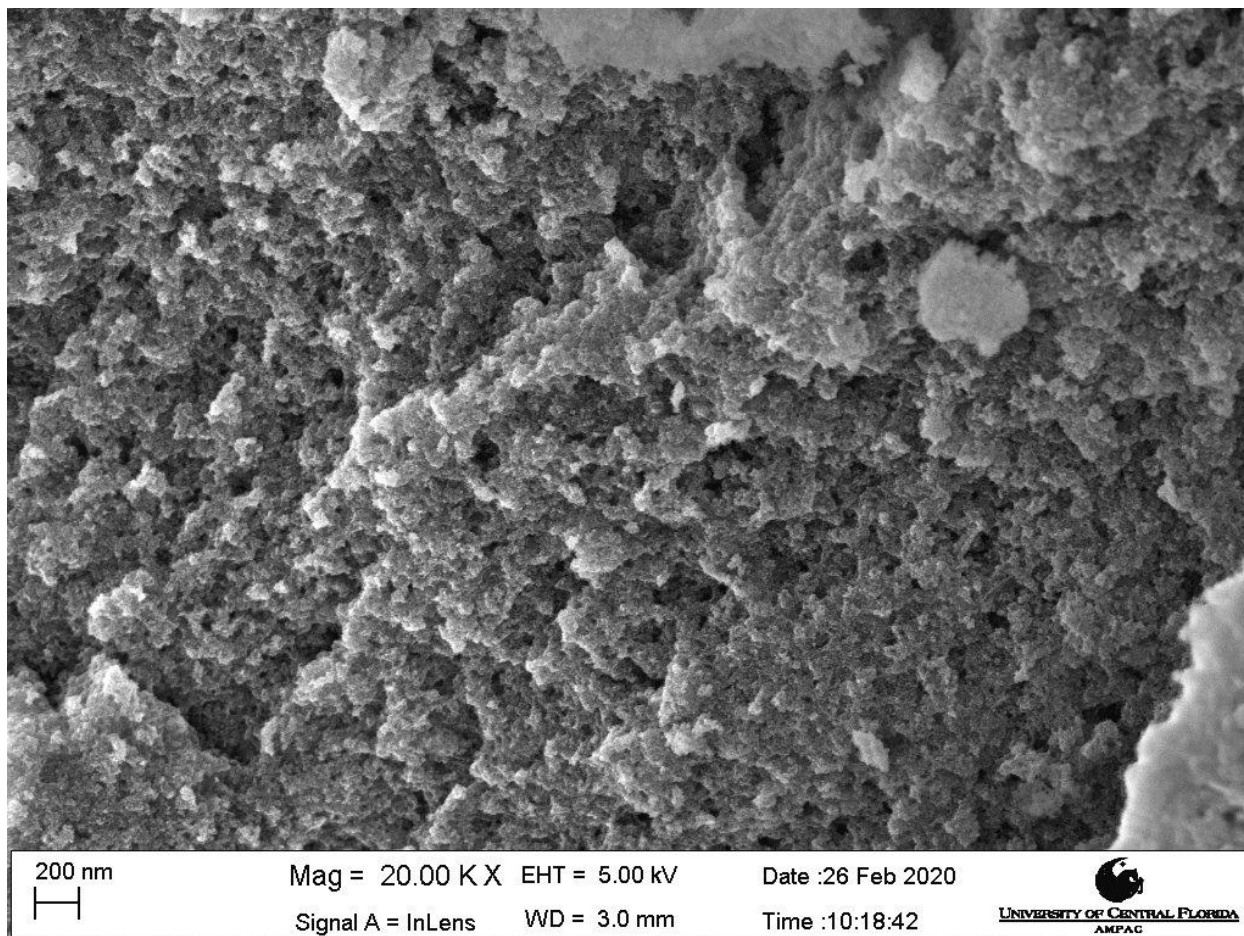


Figure 17: SEM Images of Cu/NAC-Iron Oxide.

SEM-EDS analysis of the synthesized nanomaterials showed particles composition. In Table 6, IONP weight and atom percentage is shown alongside weight and atom percent error. IONP are composed of O(K) and Fe(K) and their weight percentage was calculated to be 14.3 ± 0.2 and 85.7 ± 0.8 and their atom percentage 36.8 ± 0.4 and 63.2 ± 0.6 respectively. Also, NAC-IONP EDS analysis showed the material composition. In Table 7, NAC-IONP is composed of C(K), N(K), O(K), S(K), Fe(K) and their weight percentage is 5.4 ± 0.2 , 0.5 ± 0.3 , 24.3 ± 0.2 , 0.2 ± 0.0 , and 69.6 ± 0.7 on the other hand their atom percentage is 13.8 ± 0.6 , 1.2 ± 0.7 , 46.5 ± 0.5 , 0.2

± 0.0 , and 38.2 ± 0.4 , respectively. Additionally, Table 8 shows Cu/NAC-IONP weight and atomic percentage. Cu/NAC-IONP composed of C(K), O(K), Fe(K), and Cu(K) and their weight percentage is 1.1 ± 0.1 , 23.8 ± 0.2 , 72.1 ± 0.7 , and 3.1 ± 0.3 and their atomic percentage 3.1 ± 0.4 , 51.0 ± 0.4 , 44.3 ± 0.4 , and 1.7 ± 0.2 .

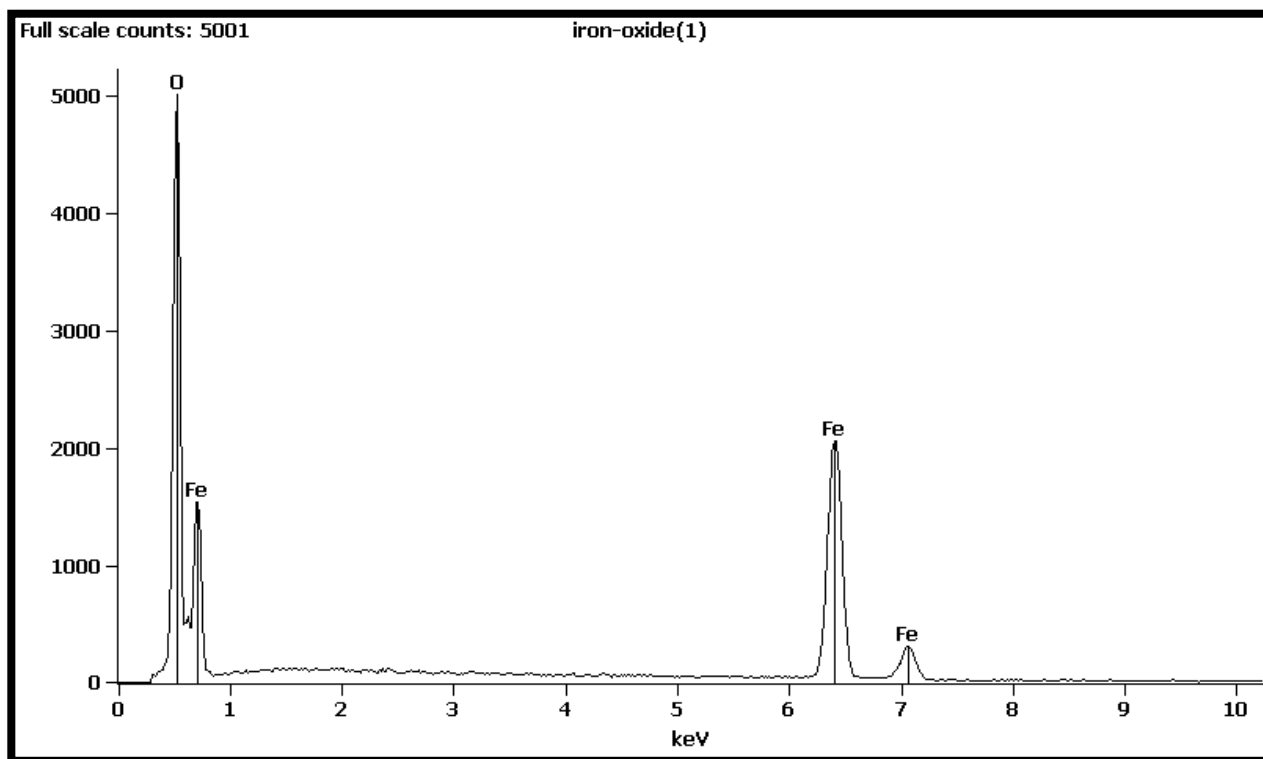


Figure 18: SEM-EDS of Iron Oxide nanoparticle.

Table 6: Semi-quantitative results of SEM-EDS analysis.

Element Line	Weight %	Weight % Error	Atom %	Atom % Error
O K	14.3	± 0.2	36.8	± 0.4
Fe K	85.7	± 0.8	63.2	± 0.6
Fe L	---	---	---	---
Total	100.0		100.0	

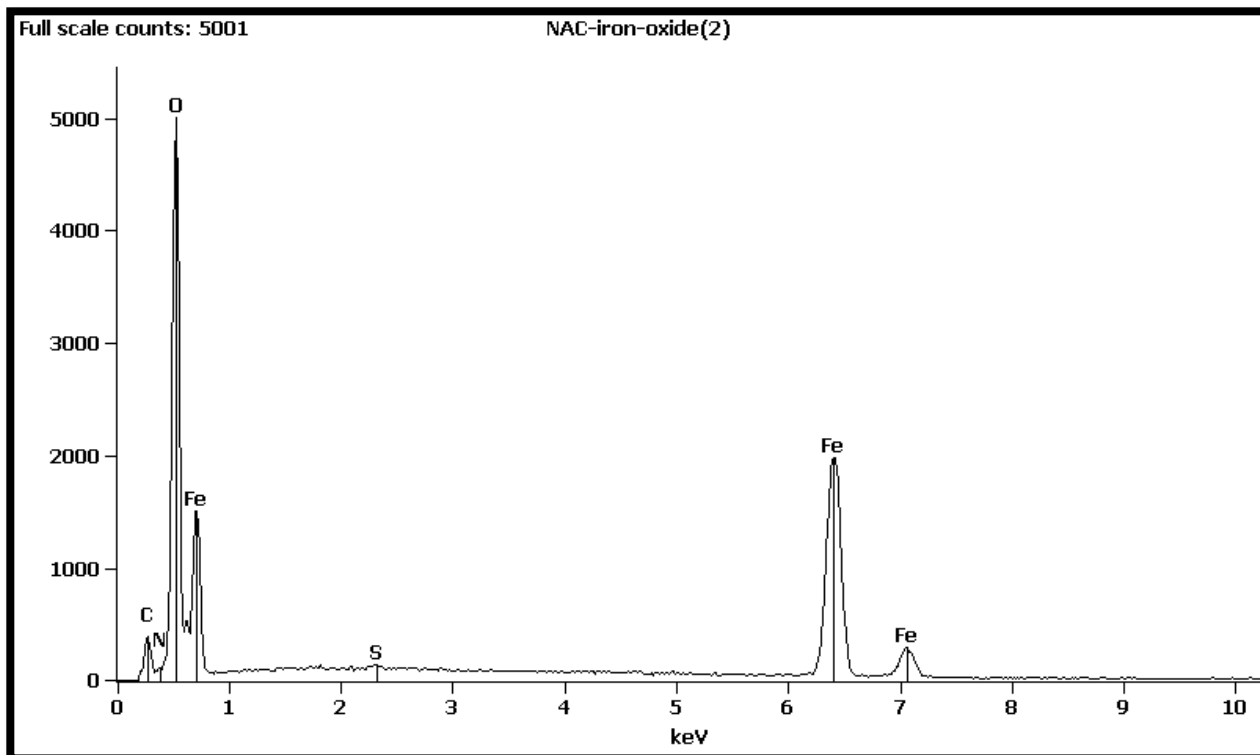


Figure 19: Energy Dispersive X-Ray Spectroscopy (EDS) of NAC-IONP.

Table 7: SEM-EDS semi-quantitative analysis of NAC-IONP.

Element Line	Weight %	Weight % Error	Atom %	Atom % Error
C K	5.4	± 0.2	13.8	± 0.6
N K	0.5	± 0.3	1.2	± 0.7
O K	24.3	± 0.2	46.5	± 0.5
S K	0.2	± 0.0	0.2	± 0.0
S L	---	---	---	---
Fe K	69.6	± 0.7	38.2	± 0.4
Fe L	---	---	---	---
Total	100.0		100.0	

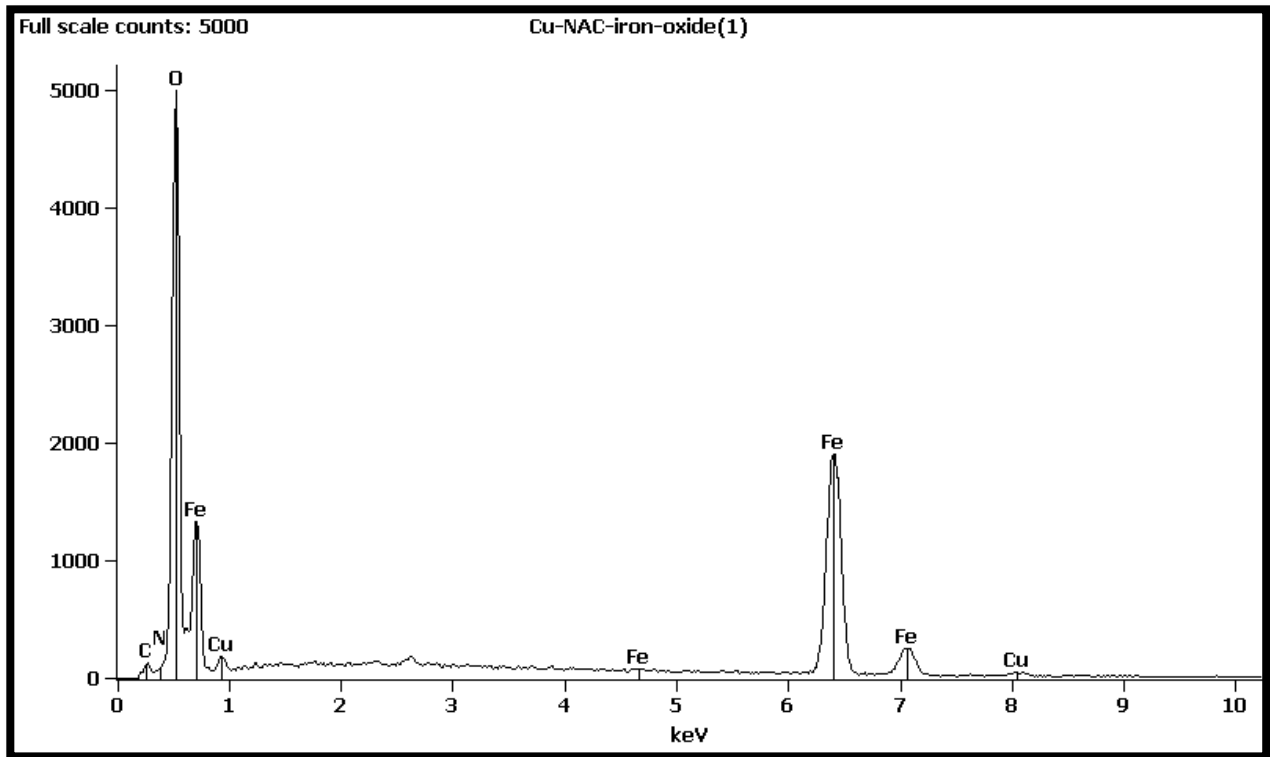


Figure 20: Energy Dispersive X-Ray Spectroscopy (EDS) of Cu/NAC-IONP.

Table 8: SEM-EDS semi-quantitative analysis of Cu/NAC-IONP

Element Line	Weight %	Weight % Error	Atom %	Atom % Error
C K	1.1	± 0.1	3.1	± 0.4
N K	0.0	---	0.0	± 0.0
O K	23.8	± 0.2	51.0	± 0.4
Fe K	72.1	± 0.7	44.3	± 0.4
Fe L	---	---	---	---
Cu K	3.1	± 0.3	1.7	± 0.2
Cu L	---	---	---	---
Total	100.0		100.0	

Antimicrobial activity was studied using ASTM E2149 published protocol with some modification. The protocol was designed to examine the antimicrobial activity of non-leaching, irregular shaped, or hydrophobic materials. This method tests the antimicrobial activity of antimicrobial material surface as it is shaken in bacterial culture suspension. Traditional methods to determine Minimum Inhibitory Concentrations (MIC) or Minimum Bactericidal Concentrations (MBC) that were previously proposed, have been found to be unfit to study these types of materials. The antimicrobial activity of Cu/NAC-IONP and NAC-IONP powder was investigated against animal infecting bacteria model system *E. coli* and plant infecting bacteria model system *P. syringae*. The studies were repeated two times and the average and standard deviation was calculated.

First, the antimicrobial activity of nanomaterial formulation against *E. coli* was determined by calculating log cell colony unit per milliliter (CFU/ml) of No treatment (NT), NAC-IONP and Cu/NAC-IONP. Figure 21 shows the mean log (CFU/ml) comparison of two Nano-treatments and control after 0hr, 4hr and 24 hr. The data shows that Log (CFU/ml) increase at every time point for NT and NAC-IONP. However, there appears to be no increase in CFU/ml for Cu/NAC-IONP. These data conclude that Cu/NAC-IONP appears to have a biostatic ability against *E. coli*.

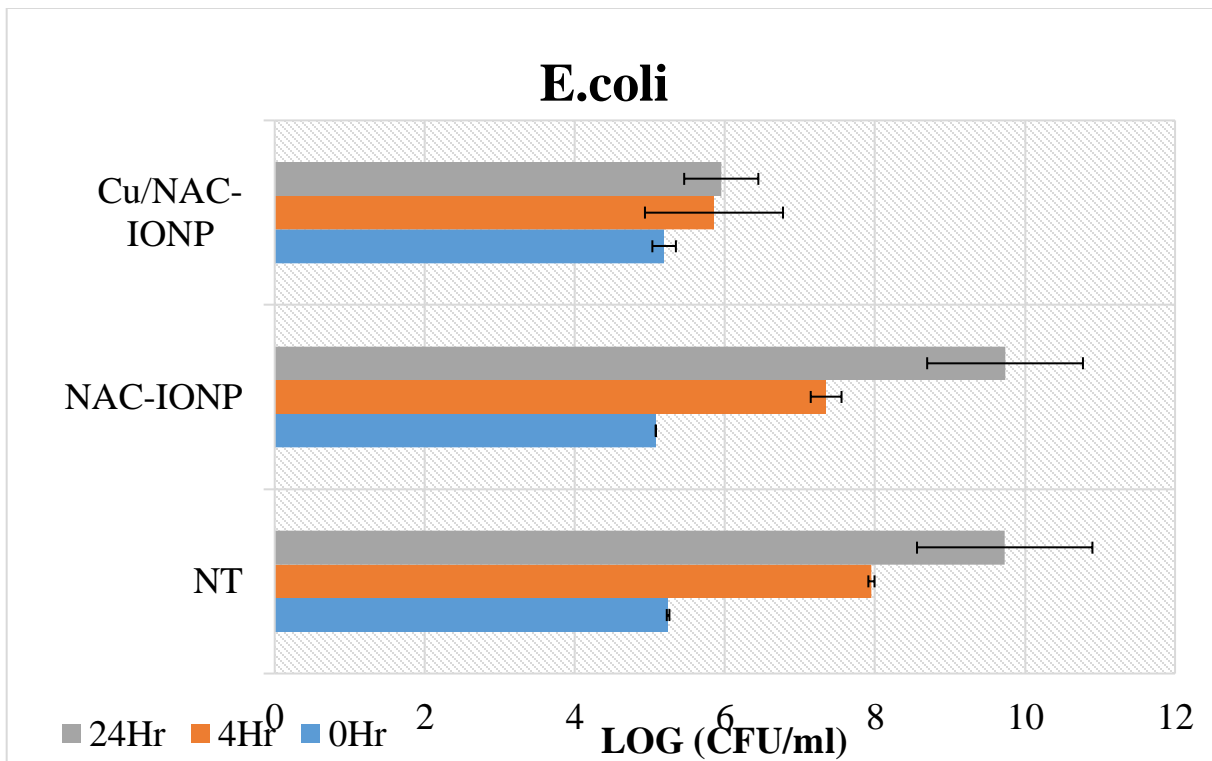


Figure 21: Examine the reduction of Cell Colony Count after 0 hours, 4 Hours and 24 Hours of NAC-Iron Oxide and Copper-NAC-iron Oxide compare with No treatment (NT). The data of nanomaterials treatment using *Escherichia coli* as animal infecting bacteria model system.

On the other hand, the same study was completed to study the antimicrobial activity of NAC-IONP and Cu/NAC-IONP against *P. syringae*. The log (CFU/ml) comparison after 0hr, 4hr, and 24hr treatment is shown in Figure 22. In the study, similar trend is observed for NT and NAC-IONP whereby the log (CFU/ml) increase at every time point. However, Cu/NAC-IONP leads reduction of log (CFU/ml) after 4hr and killing after 24hr. It has been determined that Cu/NAC-IONP demonstrate bactericidal abilities against *P. syringae* after 24hr

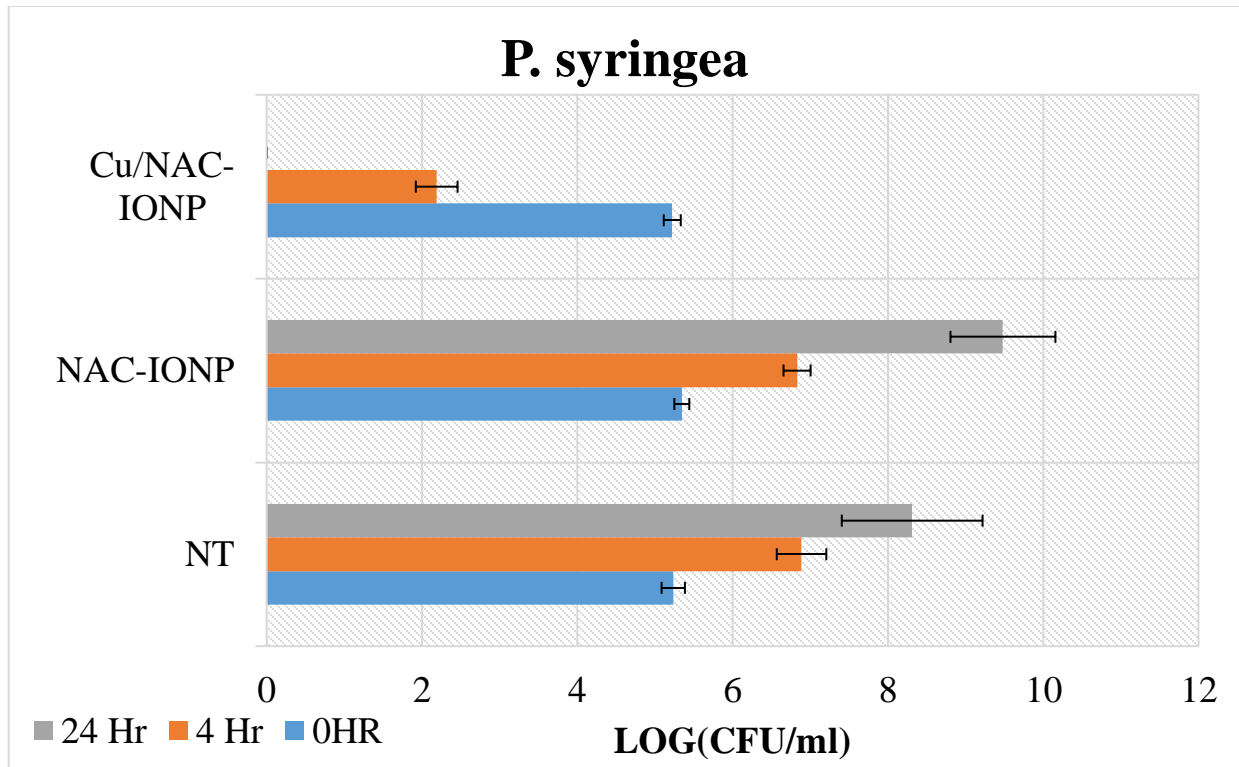


Figure 22: Examine the reduction of Cell Colony Count after 0 hours, 4 Hours and 24 Hours of NAC-Iron Oxide and Copper-NAC-iron Oxide compare with No treatment (NT) Shows the data for nanomaterials treatment using *Pseudomonas syringae* as a plant infecting bacteria model system.

A comparison of NAC-IONP and Cu/NAC-IONP mean log₁₀ bacteria reduction and reduction percentage (%) of *E.coli* and *P. syringae* are shown in Table 9. The data was obtained from Figure 24 and 25 at 24 hours shows NAC-IONP and Cu/NAC-IONP treatments against *P.syringae* have a mean log₁₀ bacteria reduction of -1.7 ± 0.2 and 8.3 ± 0.9 respectively. There appears to be no percent reduction for NAC-IONP due to the calculation of negative values. However, 100% percent reduction for Cu/NAC-IONP. The previous values demonstrate a significant bacteria reduction of Cu/NAC-IONP when compared with no reduction of NAC-

IONP. Also, the mean log₁₀ bacterial reduction calculation of *E.coli* shows -0.004 ± 0.1 and 3.8 ± 0.7 of NAC-IONP and Cu/NAC-IONP respectively. Also, the reduction percentage of *E.coli* by NAC-IONP and Cu/NAC-IONP treatment are 17.4% and 100% respectively. These values demonstrate a significantly higher antimicrobial activity of Cu/NAC-IONP when compared to NAC-IONP.

Table 9: Percent reduction of bacterial titer and the Log₁₀ bacterial titer reduction for the NAC-Iron Oxide and Cu/NAC-iron Oxide treatments after 24 hours of incubation.

Bacteria	Nanomaterials	Contact Time (hours)	Log ₁₀ Bacteria Reduction	Reduction, % (CFU/mL)
<i>P. syringae</i>	NAC-IONP	24	-1.7 ± 0.2	-
	Cu/NAC-IONP	24	8.3 ± 0.9	100
<i>E. coli</i>	NAC-IONP	24	-0.004 ± 0.1	17.4
	Cu/NAC-IONP	24	3.8 ± 0.7	100

Finally, AAS analysis of copper release in the media has been studied. After 24-hour incubation, the treatments will undergo magnetic separation and the supernatant was collected. Table 10 demonstrate the calculated copper release in the two different growth media for *E.coli* and *P. syringea* growth. *E.coli* antimicrobial study utilized Luria-Bertani broth with a pH of 7.09 and incubated at 37°C. Figure 23 shows the copper concentration in the media after 24hr was calculated to be 95.8 ± 7.2 . On the other hand, in the antimicrobial study for *P.syrinega* a nutrient broth with pH 7.11 was used and the bacterial suspensions was incubated at 28°C. Figure 24 shows copper concentration in the media after 24 hours was calculated to be 43.9 ± 1.89 . The differences in Copper release has been attributed to the incubation temperature needed for the bacteria to grow. *E. coli* bacteria culture was incubated at 37°C while *P. syringea* bacteria

culture was incubated 28°C. The higher temperature increase copper release by about 52%. This analysis has unwrapped a new possibility for the future development of this materials with targeted controlled release of copper.

Table 10: Effects of temperature on the Copper release amount after 24 hours of incubation.

	<i>P. syringea</i> (Cu-ppm)	<i>E. coli</i> (Cu-ppm)
Media(pH)	Nutrient Broth (7.11)	Luria-Bertani(LB) Broth (7.09)
Incubation Temperature (C ⁰)	28	37
No treatment (NT)	--	--
NAC-IONP	--	--
Cu/NAC-IONP	43.9± 1.89	95.8± 7.2

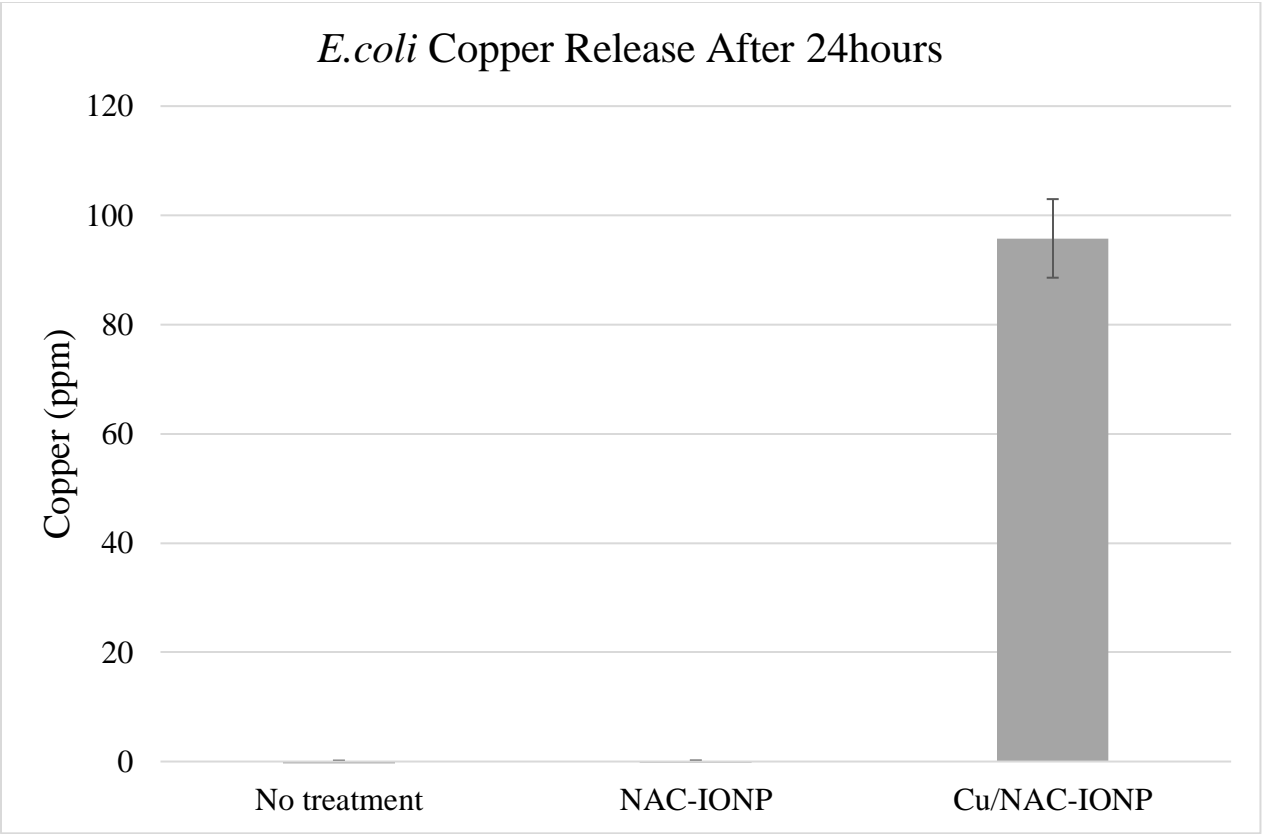


Figure 23: AAS study of Copper release in LB media.

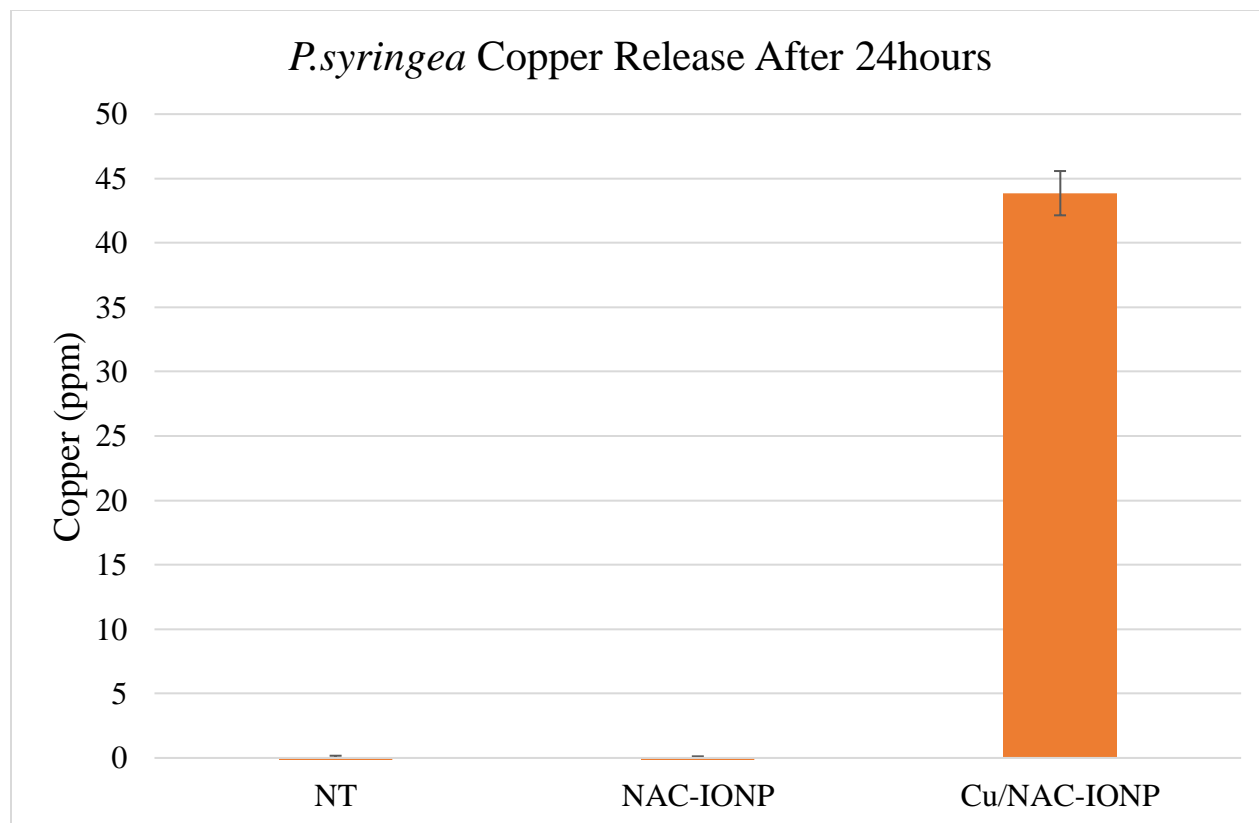


Figure 24: AAS study of Copper Release in NB media.

Magnetic nanoparticles are being studied for hyperthermia treatment. Magnetic Iron oxide nanoparticles can be injected into tumor and the particles generate heat when alternating magnetic field is applied (Giustini et al., 2010; Thiesen & Jordan, 2008). As well as, copper particles have been investigated for biomedical application such as anti-tumor treatment. Other studies have shown copper nanoparticle being used as a potential apoptosis inducing agent, and that copper oxide nanoparticles with or without chemical modification have been widely used in many different cancers such as, kidney lung, liver, brain, breast, prostate, and eye (Verma &

Kumar, 2019). Therefore, the potential of Cu/NAC-IONP as anti-tumor agent should be investigated in future studies.

CHAPTER FIVE: CONCLUSION

We have successfully developed and optimized a synthesis procedure for Copper/N-acetylcysteine Iron Oxide nanoparticles. Several characterization techniques such as AAS, DLS, FTIR, SEM, SEM-EDS and XPS have been used to study size, size distribution, composition and behavior in solution and dry state. Data support that NAC is able to conjugate Cu to IONP. SEM results show that primary particles appear to be spherical, somewhat uniform but they remain in highly aggregated state. DLS data demonstrate the high Z-average which supports the aggregation and coating adsorption. There is no significant difference between NAC-IONP and Cu/NAC-IONP FTIR signature peaks, this suggest that NAC interaction with IONP is likely through ionic interaction. The antimicrobial activity of Cu/NAC-IONP nanocomposite shows higher CFU/ml reduction when compared with NAC-IONP and no treatment. This suggests that copper antimicrobial activity is preserved in the nanocomposite. Finally, AAS study showed that Cu ion release is increased with the increase in incubation temperature.

APPENDIX: SUPPLEMENTARY INFORMATION

XPS analysis was completed to determine the presence of copper and its metallic configuration in the Nano-formulations to better understand the mode of killing. However, since copper concentration was low, copper peaks could not clearly distinguish from similar iron peaks. Nevertheless, the data was graphed using Origin2018b, and all the peaks were labeled. Figure 21 shows the XPS survey spectrum of IONP and the following peaks were labeled Fe3p, Fe3s, C1s, O1s, Fe2p3, Fe2p1, FeLM2 Fe2s, and O KL1 at 56,94, 285, 530, 712, 726, 783, 843, 976eV respectively. Also, Figure 22 shows NAC-IONP XPS survey C k11, O K12, Ok11, Fe lm6, Fe2s, Fe Lm2, Fe 2 p1, Fe 2p3, O1s, C1s, Fe3s, Fe3p at 1222, 999, 974, 897, 850, 787, 726, 711, 531, 285, 100, and 55 eV. Figure 23 shows the Cu/NAC-IONP has peaks labeled as O KL2, O KL, FeLM8, Fe lm6, Fe2s, Fe Lm2, Fe 2 p1, Cu LM5, O1s, C1s, Fe3s, and Fe3p at 995, 974, 932, 902, 845, 784, 725, 711, 530, 286, 94, and 55.

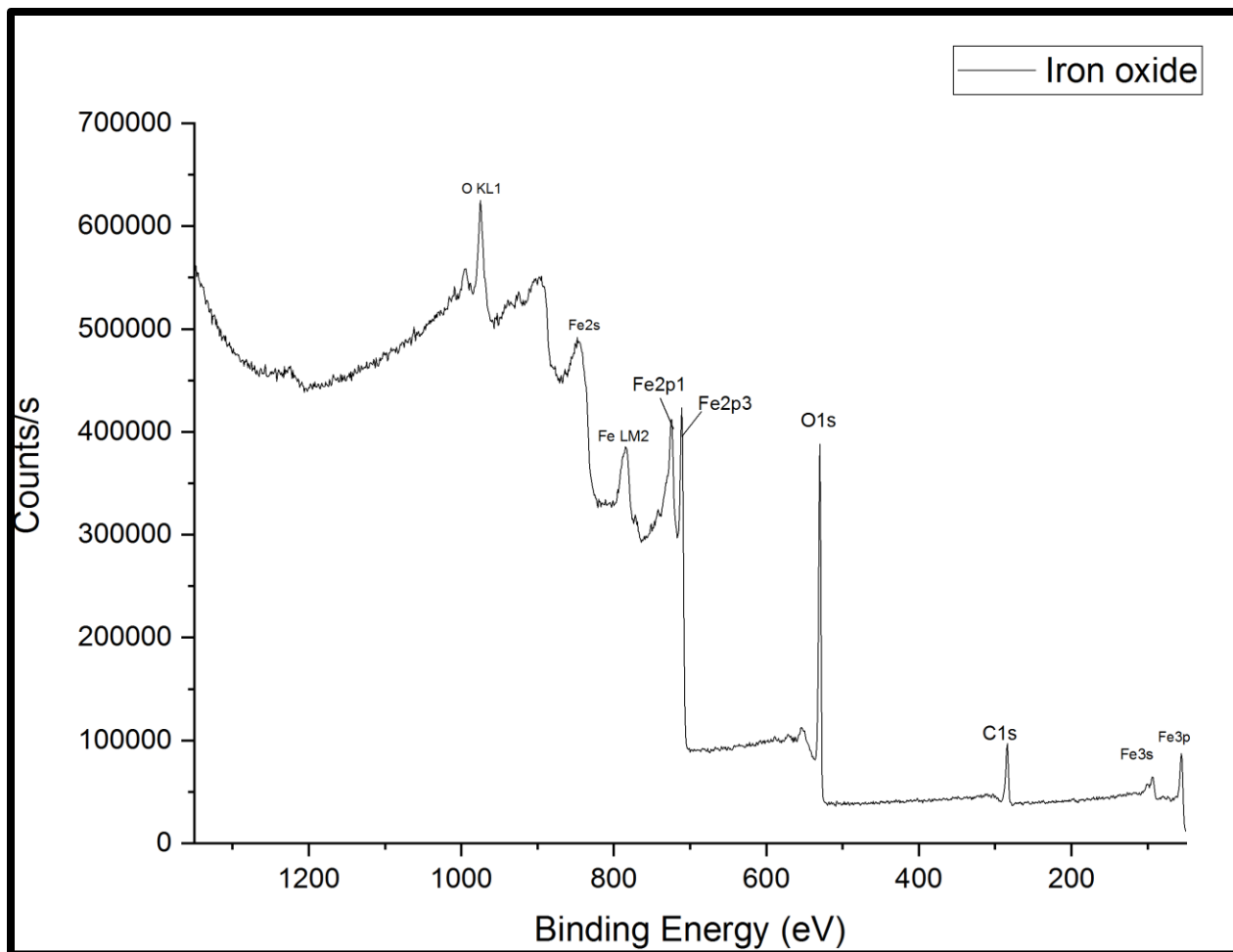


Figure 25: An XPS survey spectrum of IONP.

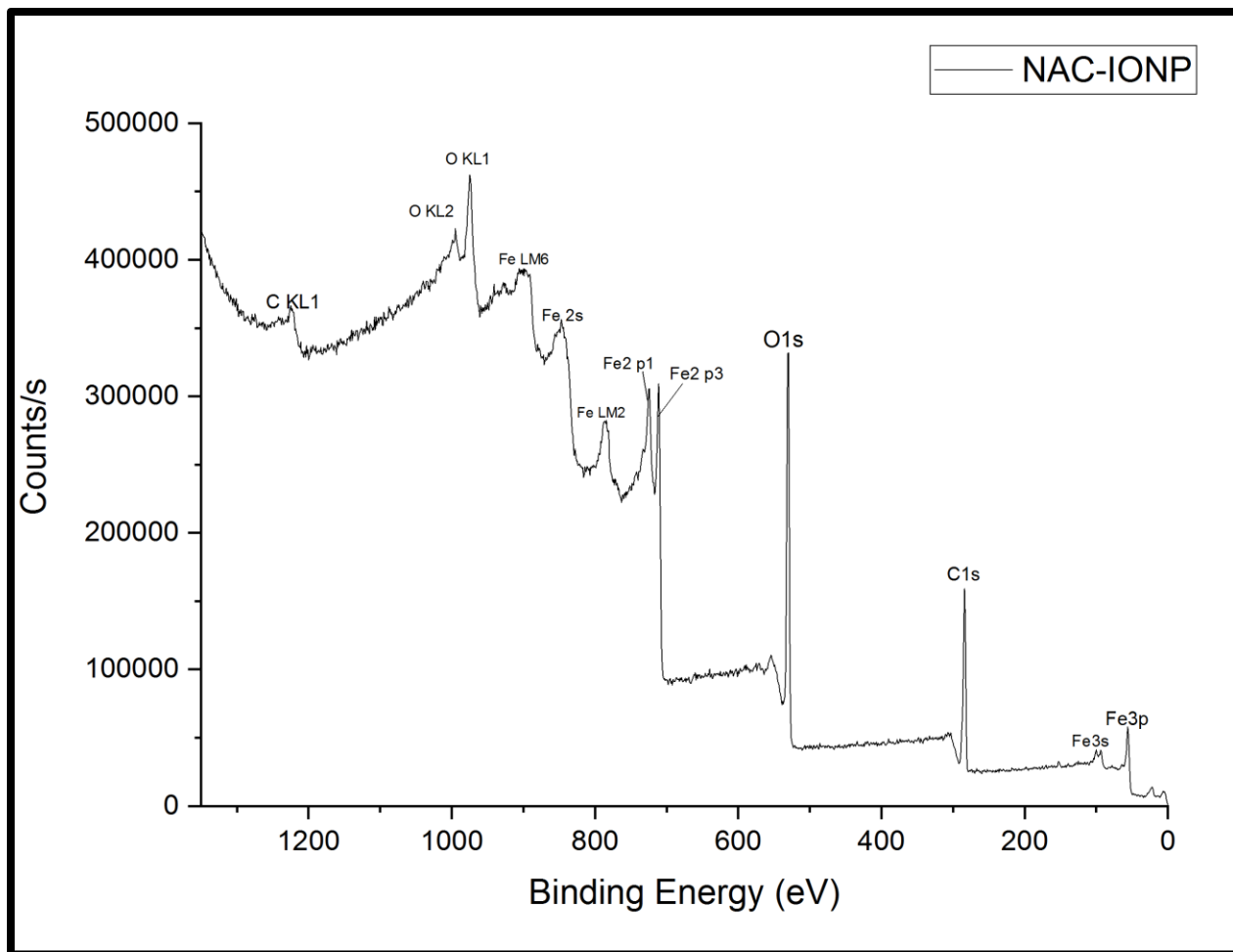


Figure 26: An XPS survey spectrum of NAC-IONP

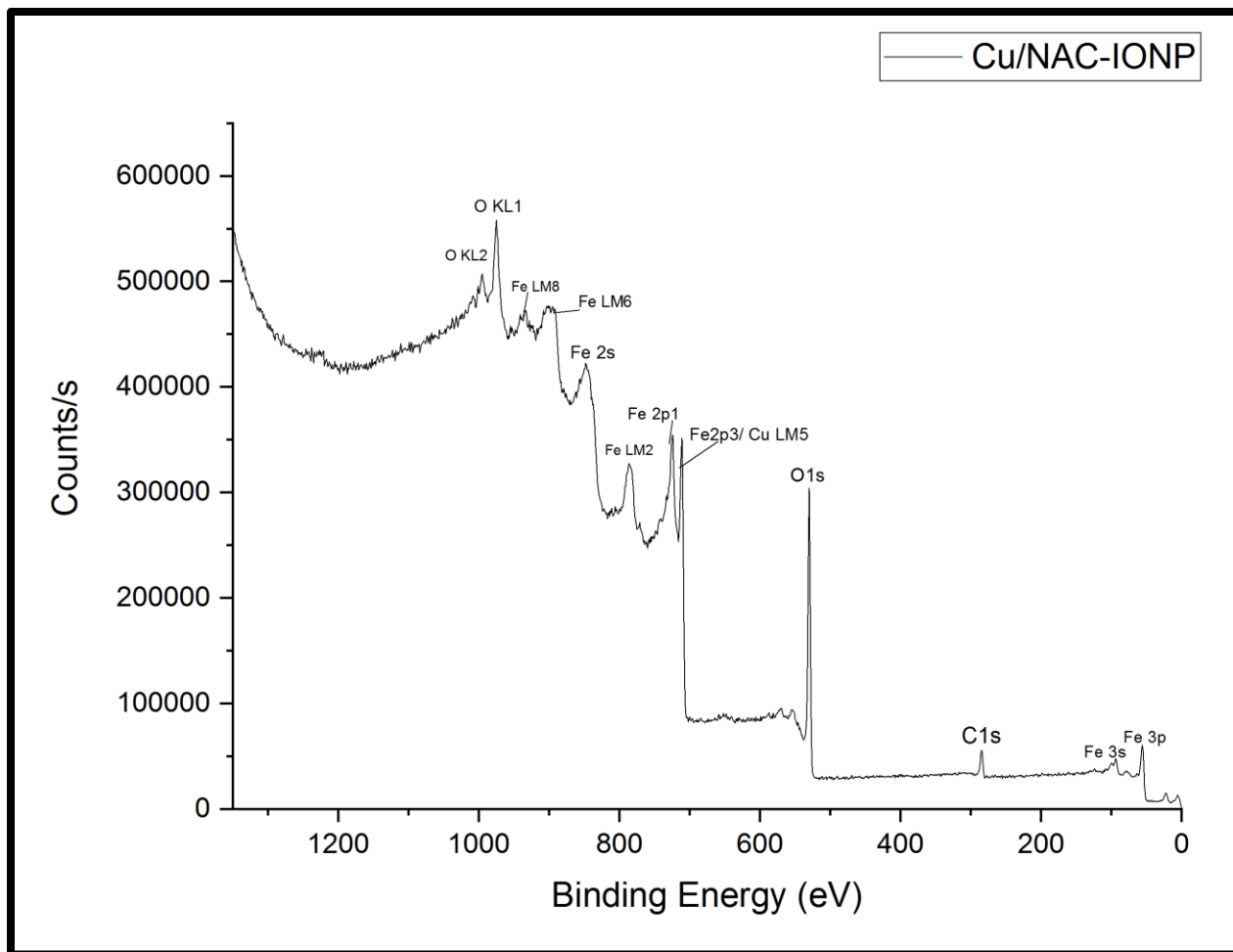


Figure 27: An XPS survey spectrum of Cu/NAC-IONP

LIST OF REFERENCES

- Ali, A., Hira Zafar, M. Z., ul Haq, I., Phull, A. R., Ali, J. S., & Hussain, A. (2016). Synthesis, characterization, applications, and challenges of iron oxide nanoparticles. *Nanotechnology, science and applications*, 9, 49.
- Ali, M. A., Rehman, I., Iqbal, A., Din, S., Rao, A. Q., Latif, A., . . . Husnain, T. (2014). Nanotechnology, a new frontier in Agriculture. *Adv life sci*, 1(3), 129-138.
- Cortajarena, A. L., Ortega, D., Ocampo, S. M., Gonzalez-García, A., Couleaud, P., Miranda, R., . . . Ayuso-Sacido, A. (2014). Engineering iron oxide nanoparticles for clinical settings. *Nanobiomedicine*, 1(Godište 2014), 1-2.
- E2149–13a, A. (2013). *Standard test method for determining the antimicrobial activity of antimicrobial agents under dynamic contact conditions*.
- Fang, Y., & Ramasamy, R. P. (2015). Current and prospective methods for plant disease detection. *Biosensors*, 5(3), 537-561.
- Ferrari, M. (2005). Cancer nanotechnology: opportunities and challenges. *Nature reviews cancer*, 5(3), 161-171.
- Flora, S. J. (2009). Structural, chemical and biological aspects of antioxidants for strategies against metal and metalloid exposure. *Oxidative medicine and cellular longevity*, 2.
- Giustini, A. J., Petryk, A. A., Cassim, S. M., Tate, J. A., Baker, I., & Hoopes, P. J. (2010). Magnetic nanoparticle hyperthermia in cancer treatment. *Nano Life*, 1(01n02), 17-32.

- Graham, J., Johnson, E., Myers, M., Young, M., Rajasekaran, P., Das, S., & Santra, S. (2016). Potential of nano-formulated zinc oxide for control of citrus canker on grapefruit trees. *Plant disease*, *100*(12), 2442-2447.
- Grass, G., Rensing, C., & Solioz, M. (2011). Metallic copper as an antimicrobial surface. *Applied and environmental microbiology*, *77*(5), 1541-1547.
- Gupta, A. K., & Gupta, M. (2005). Synthesis and surface engineering of iron oxide nanoparticles for biomedical applications. *biomaterials*, *26*(18), 3995-4021.
- Huang, H.-Y., Shieh, Y.-T., Shih, C.-M., & Twu, Y.-K. (2010). Magnetic chitosan/iron (II, III) oxide nanoparticles prepared by spray-drying. *Carbohydrate Polymers*, *81*(4), 906-910.
- Kalantar-zadeh, K., & Fry, B. (2007). *Nanotechnology-enabled sensors*: Springer Science & Business Media.
- Kalantar-zadeh, K., & Fry, B. (2008). Characterization techniques for nanomaterials. *Nanotechnology-Enabled Sensors*, 211-281.
- Lauren, S., Forge, D., Port, M., Roch, A., Robic, C., Elst, L. V., & Muller, R. N. r. m. u. a. b. (2008). Magnetic Iron Oxide Nanoparticles: Synthesis, Stabilization, Vectorization, Physicochemical Characterizations, and Biological Applications. *Chemical Reviews*, *108*(6), 2064-2110. doi:10.1021/cr068445e
- Leamy, P. J. (2003). *Preparation, Characterization, and in Vitro Testing of Poly (lactide-co-glycolide) and Dextran Magnetic Microspheres for in Vivo Applications*: University of Florida.

- Mokhtari, V., Afsharian, P., Shahhoseini, M., Kalantar, S. M., & Moini, A. (2017). A review on various uses of N-acetyl cysteine. *Cell Journal (Yakhteh)*, 19(1), 11.
- Muranaka, L. S., Giorgiano, T. E., Takita, M. A., Forim, M. R., Silva, L. F., Coletta-Filho, H. D., . . . de Souza, A. A. (2013). N-Acetylcysteine in agriculture, a novel use for an old molecule: focus on controlling the plant–pathogen *Xylella fastidiosa*. *PLoS One*, 8(8), e72937.
- Namduri, H., & Nasrazadani, S. (2008). Quantitative analysis of iron oxides using Fourier transform infrared spectrophotometry. *Corrosion Science*, 50(9), 2493-2497.
- Naranjo, E., Merfa, M. V., Santra, S., Ozcan, A., Johnson, E., Cobine, P. A., & De La Fuente, L. (2020). Zinkicide® is a ZnO-based nano-formulation with bactericidal activity against *Liberibacter crescens* in batch cultures and in microfluidic chambers simulating plant vascular systems. *Applied and environmental microbiology*.
- Ozcan, A. (2019). Advanced Multifunctional Bactericides for Crop Protection: A New Strategy to Reduce Cu Pesticide Footprint in the Environment.
- Park, J., An, K., Hwang, Y., Park, J.-G., Noh, H.-J., Kim, J.-Y., . . . Hyeon, T. (2004). Ultra-large-scale syntheses of monodisperse nanocrystals. *Nature materials*, 3(12), 891.
- Peshin, R., & Dhawan, A. K. (2009). *Integrated Pest Management: Volume 1: Innovation-Development Process* (Vol. 1): Springer Science & Business Media.
- Prodan, A. M., Iconaru, S. L., Ciobanu, C. S., Chifiriuc, M. C., Stoicea, M., & Predoi, D. (2013). Iron oxide magnetic nanoparticles: characterization and toxicity evaluation by in vitro and in vivo assays. *journal of Nanomaterials*, 2013.

- Rai, M., & Ingle, A. (2012). Role of nanotechnology in agriculture with special reference to management of insect pests. *Applied microbiology and biotechnology*, 94(2), 287-293.
- Santra, S., & Huang, Z. (2020). Antimicrobial Magnesium Hydroxide Nanoparticles as an Alternative to Cu Biocide for Crop Protection. In: US Patent App. 16/659,490.
- Santra, S., Tapeç, R., Theodoropoulou, N., Dobson, J., Hebard, A., & Tan, W. (2001). Synthesis and characterization of silica-coated iron oxide nanoparticles in microemulsion: the effect of nonionic surfactants. *Langmuir*, 17(10), 2900-2906.
- Saraswathy, A., Nazeer, S. S., Jeevan, M., Nimi, N., Arumugam, S., Harikrishnan, V. S., . . . Jayasree, R. S. (2014). Citrate coated iron oxide nanoparticles with enhanced relaxivity for in vivo magnetic resonance imaging of liver fibrosis. *Colloids and Surfaces B: Biointerfaces*, 117, 216-224.
- Sigmund, W., El-Shall, H., Shah, D. O., & Moudgil, B. M. (2008). *Particulate systems in nano- and biotechnologies*: CRC Press.
- Song, C., Sun, W., Xiao, Y., & Shi, X. (2019). Ultrasmall iron oxide nanoparticles: synthesis, surface modification, assembly, and biomedical applications. *Drug Discovery Today*, 24(3), 835-844.
- Sun, H., Yang, B., Cui, E., & Liu, R. (2014). Spectroscopic investigations on the effect of N-acetyl-L-cysteine-capped CdTe Quantum Dots on catalase. *Spectrochimica Acta Part A: Molecular and Biomolecular Spectroscopy*, 132, 692-699.
- Thiesen, B., & Jordan, A. (2008). Clinical applications of magnetic nanoparticles for hyperthermia. *International journal of hyperthermia*, 24(6), 467-474.

- Verma, N., & Kumar, N. (2019). Synthesis and biomedical applications of copper oxide nanoparticles: an expanding horizon. *ACS Biomaterials Science & Engineering*, 5(3), 1170-1188.
- Wiegand, I., Hilpert, K., & Hancock, R. E. (2008). Agar and broth dilution methods to determine the minimal inhibitory concentration (MIC) of antimicrobial substances. *Nature protocols*, 3(2), 163.
- Xin, X.-F., Kvitko, B., & He, S. Y. (2018). *Pseudomonas syringae*: what it takes to be a pathogen. *Nature Reviews Microbiology*, 16(5), 316.
- Young, M., Ozcan, A., Myers, M. E., Johnson, E. G., Graham, J. H., & Santra, S. (2017). Multimodal generally recognized as safe ZnO/nanocopper composite: A novel antimicrobial material for the management of citrus phytopathogens. *Journal of agricultural and food chemistry*, 66(26), 6604-6608.
- Young, M., Ozcan, A., Rajasekaran, P., Kumrah, P., Myers, M. E., Johnson, E., . . . Santra, S. (2018). Fixed-Quat: An Attractive Nonmetal Alternative to Copper Biocides against Plant Pathogens. *Journal of agricultural and food chemistry*, 66(50), 13056-13064.
- Young, M., & Santra, S. (2014). Copper (Cu)–Silica nanocomposite containing valence-engineered Cu: a new strategy for improving the antimicrobial efficacy of Cu biocides. *Journal of agricultural and food chemistry*, 62(26), 6043-6052.